JOURNAL OF PETROLOGY | VOLUME 47 | NUMBER 3 | PAGES 595–629 | 2006 | doi:10.1093/petrology/egi087

The Petrology and Geochemistry of Oto-Zan Composite Lava Flow on Shodo-Shima Island, SW Japan: Remelting of a Solidified High-Mg Andesite Magma

Y. TATSUMI[1]*, T. SUZUKI[1], H. KAWABATA[1], K. SATO[1], T. MIYAZAKI[1], Q. CHANG[1], T. TAKAHASHI[1], K. TANI[1], T. SHIBATA[2] AND M. YOSHIKAWA[2]

[1]INSTITUTE FOR RESEARCH ON EARTH EVOLUTION (IFREE), JAPAN AGENCY FOR MARINE-EARTH SCIENCE AND TECHNOLOGY (JAMSTEC), YOKOSUKA 237-0061, JAPAN

[2]INSTITUTE FOR GEOTHERMAL SCIENCES, KYOTO UNIVERSITY, BEPPU 974-0907, JAPAN

RECEIVED DECEMBER 16, 2004; ACCEPTED OCTOBER 20, 2005
ADVANCE ACCESS PUBLICATION DECEMBER 8, 2005

*The Oto-Zan lava in the Setouchi volcanic belt is composed of phenocryst-poor, sparsely plagioclase-phyric andesites (sanukitoids) and forms a composite lava flow. The phenocryst assemblages and element abundances change but Sr–Nd–Pb isotopic compositions are constant throughout the lava flow. The sanukitoid at the base is a high-Mg andesite (HMA) and contains Mg- and Ni-rich olivine and Cr-rich chromite, suggesting the emplacement of a mantle-derived hydrous (~7 wt % H_2O) HMA magma. However, Oto-Zan sanukitoids contain little H_2O and are phenocryst-poor. The liquid lines of descent obtained for an Oto-Zan HMA at 0·3 GPa in the presence of 0·7–2·1 wt % H_2O suggest that mixing of an HMA magma with a differentiated felsic melt can reasonably explain the petrographical and chemical characteristics of Oto-Zan sanukitoids. We propose a model whereby a hydrous HMA magma crystallizes extensively within the crust, resulting in the formation of an HMA pluton and causing liberation of H_2O from the magma system. The HMA pluton, in which interstitial rhyolitic melts still remain, is then heated from the base by intrusion of a high-*T *basalt magma, forming an H_2O-deficient HMA magma at the base of the pluton. During ascent, this secondary HMA magma entrains the overlying interstitial rhyolitic melt, resulting in variable self-mixing and formation of a zoned magma reservoir, comprising more felsic magmas upwards. More effective upwelling of more mafic, and hence less viscous, magmas through a propagated vent finally results in the emplacement of the composite lava flow.*

KEY WORDS: *high-Mg andesite; sanukitoid; composite lava; solidification; remelting*

INTRODUCTION

The majority of andesites that typify subduction zone magmatism are derived from parental basaltic magmas through variable differentiation processes such as fractional crystallization, mixing with felsic magmas, crustal contamination and anatexis of pre-existing basaltic crustal materials (e.g. Gill, 1981; Hildreth, 1981; Sakuyama, 1981; Hunter, 1998; Temel *et al.*, 1998; Couch *et al.*, 2001; Tatsumi *et al.*, 2002; Grove *et al.*, 2003). On the other hand, mantle-derived, primary andesitic magmas also exist in arcs. Such unusual andesites are referred to as high-Mg andesites (HMAs), as they are characterized by high MgO contents and/or Mg-number (= 100 × Mg/(Mg + Fe)) and are in equilibrium with Mg-rich mantle minerals. The occurrence of HMAs has been reported, for example, from the Bonin Islands (Kuroda *et al.*, 1978), Baja California (Saunders *et al.*, 1987), Piip volcano in W Aleutians (Yogodzinski *et al.*, 1994), and the Setouchi volcanic belt in SW Japan (Tatsumi & Ishizaka, 1981).

High-pressure melting experiments on both simple and natural peridotite systems (e.g. Kushiro, 1969; Hirose,

*Corresponding author. E-mail: tatsumi@jamstec.go.jp

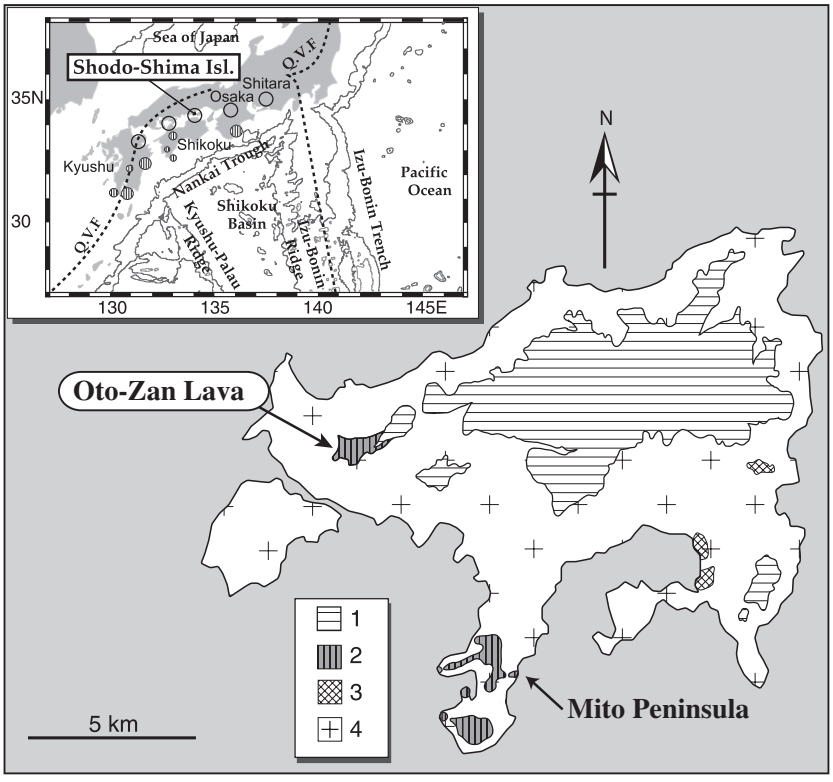

Fig. 1. Tectonic setting of the Setouchi volcanic belt (inset) and a simplified geological map of Shodo-Shima Island after Tatsumi (1983). The Setouchi volcanic belt (open circles) and coeval Outer Zone felsic complexes (hatched circles) are distributed to the trench side of the Quaternary volcanic front (QVF) of the SW Japan arc. Setouchi volcanic rocks on Shodo-Shima Island, which cover granitic basement (4), are divided into two groups, the Kankakei (1, porphyritic andesite; 2, sanukitoid) and the Uchinomi (3) formations in descending order. The Oto-Zan lava flow forms the lowermost part of the Kankakei Formation. Bathymetric contours are given in 2000 m intervals.

1997) have established that partial melting of upper mantle peridotite under hydrous conditions is a possible mechanism for HMA magma production. It has been further demonstrated that some HMAs are multiply saturated with peridotitic phases under hydrous conditions at mantle pressures (e.g. Kushiro & Sato, 1978; Tatsumi, 1981, 1982; Umino & Kushiro, 1989; van der Laan *et al.*, 1989). These experimental results led Crawford *et al.* (1989) and Tatsumi & Maruyama (1989) to the conclusion that the direct overprinting of aqueous fluids released from the subducting lithosphere onto the mantle wedge is a likely mechanism for HMA magma generation. However, this rather simple process is not the only way to attain equilibration between hydrous HMA magmas and mantle peridotite. A process involving partial melting of subducting lithosphere and subsequent reaction of such hydrous felsic slab melts with mantle wedge peridotite has been widely accepted as a likely mechanism for the generation of hydrous HMA magmas (Kay, 1978; Pearce *et al.*, 1992; Yogodzinski *et al.*, 1994; Kelemen, 1995; Shimoda *et al.*, 1998; Tatsumi, 2001; Hanyu *et al.*, 2002). Geochemical modelling suggests that the observed Sr–Nd–Pb–Hf isotopic signatures of HMAs can be reasonably and quantitatively understood by this process (Tatsumi & Hanyu, 2003).

HMA magmas contain larger amounts of H_2O than basalt magmas when the magma left the mantle (e.g. Tatsumi, 1982), and will be oversaturated with H_2O during ascent, causing extensive crystallization. It is thus likely that HMAs are rich in phenocrysts and contain a larger amount of H_2O than other arc basaltic magmas, as observed for boninites (e.g. Dobson & O'Neil, 1987; Umino & Kushiro, 1989; Sobolev & Danyushevsky, 1994). In contrast, HMAs in the Setouchi volcanic belt are rather aphyric and poor in H_2O (e.g. Tatsumi & Ishizaka, 1981, 1982*a*, 1982*b*). This apparent paradox needs to be assessed.

In this paper, the petrography and geochemistry of a single composite lava flow that contains HMA at its base are presented. The origin of the composite lava flow and a likely mechanism that may overcome the above paradox will be discussed.

GEOLOGICAL SETTINGS

The Oto-Zan lava flow is located on Shodo-Shima Island, SW Japan (Fig. 1). The current SW Japan arc is

being built by subduction of the Philippine Sea plate from the Nankai Trough beneath the Eurasian plate (Fig. 1). The Quaternary volcanic front is located ~100 km above the top of the subducting slab, as is the case for most arc–trench systems (Tatsumi & Eggins, 1995). Miocene igneous rocks are distributed in the present fore-arc region of the SW Japan arc. In the near-trench region of this arc (the Outer Zone), felsic volcano-plutonic complexes were emplaced at 14 ± 1 Ma (Shibata, 1978; Sumii, 2000) into a Cretaceous to Miocene accretionary prism or subduction complex (Fig. 1). Synchronous with this near-trench magmatism, i.e. at 13·7 ± 1·0 Ma (Tatsumi *et al.*, 2001, 2003), volcanism took place in the Setouchi volcanic belt (Fig. 1). The zonal arrangement of Miocene magmatism parallel to the arc–trench system suggests a contribution from the plate subduction to the formation of these magmatic belts.

Miocene magmatism, both in the Setouchi region and the Outer Zone of the SW Japan arc, was largely synchronous with the timing of a 40–50° clockwise rotation of the arc sliver at 14–16 Ma that was caused by the opening of the Sea of Japan back-arc basin (Otofuji *et al.*, 1991). The Shikoku Basin, situated to the south of the SW Japan arc (Fig. 1), is also a back-arc basin that was created behind the Izu–Bonin–Mariana arc by rifting at 30–15 Ma (Okino *et al.*, 1994, 1998, 1999). It is thus inferred that the southward drift of the SW Japan arc in association with the clockwise rotation of the SW Japan arc sliver resulted in subduction of the young (<16 my) oceanic lithosphere of the Shikoku Basin. Such an unusual tectonic setting and accompanying thermal conditions could have caused slab melting to produce magmatism unusually close to the trench in the Miocene SW Japan arc (Furukawa & Tatsumi, 1999; Tatsumi & Hanyu, 2003).

Rocks distributed in the Setouchi volcanic belt include phenocryst-poor, sparsely plagioclase-phyric andesites (including HMAs) and basalts referred to as sanukitoids (Tatsumi & Ishizaka, 1981), porphyritic and plagioclase-phyric 'normal' calc-alkalic andesites, garnet-bearing dacites/rhyolites, and pitchstones. These volcanic rocks are collectively distributed on Shodo-Shima Island, which is located to the NE of Shikoku (Fig. 1). The older Setouchi volcanic rocks on the island (Uchinomi Formation), which cover basement granites and gneisses, are composed of felsic lava flows, lava domes, sheets, dykes and volcaniclastic rocks, whereas the younger group (Kankakei Formation) consists of volcanic rocks of intermediate to mafic composition (Fig. 1). K–Ar dates for Setouchi volcanics on Shodo-Shima Island (Tatsumi *et al.*, 2001) yield mean ages of 12·82 ± 0·12 and 13·78 ± 0·17 Ma for the Kankakei and Uchinomi Formations, respectively, which is consistent with the stratigraphic relations. Tatsumi (1983) suggested that most lavas and volcaniclastics on Shodo-Shima Island were emplaced under subaqueous conditions, as they show typical water-chilled structures with cracks perpendicular to the block surface.

The Oto-Zan lava flow, which is located in the western part of the island, forms the lowermost part of the Kankakei Formation and directly covers basement rocks (Fig. 1). The maximum thickness of this lava flow is ~100 m. Although the lowermost part of the lava flow forms a lava clinker consisting of water-chilled volcanic breccias and volcaniclastics, the main part of the lava flow is massive. Importantly, no flow unit boundary is observed within the lava flow, suggesting that the Oto-Zan lava is a single lava flow.

ANALYTICAL AND EXPERIMENTAL METHODS

Chemical analyses

Major and trace element (Ni, Cu, Zn, Rb, Sr, Y, Zr, Nb, Ba, Pb and Th) compositions were measured using RIGAKU® Simaltics 3512 and Rix 3000 X-ray fluorescence (XRF) spectrometers on fused glass beads and pressed powder pellets, respectively. Detailed analytical procedures have been described by Goto & Tatsumi (1994, 1996) and Tani *et al.* (2005).

Rock samples for trace elements (ICP-MS) and Sr–Nd–Pb isotope analysis were crushed to coarse chips (<0·5 mm^3) and fresh pieces were hand-picked. To avoid surface contamination, the rock chips were washed with ethanol and then leached with 0·5M HCl at room temperature for 1 h. Finally, the chips were rinsed three times with Milli-Q water. The chips were ground to less than 200 mesh size using a vibration mill made of alumina ceramic.

Concentrations of rare earth and 14 other trace elements (Sc, Rb, Sr, Y, Zr, Nb, Cs, Ba, Hf, Ta, Tl, Pb, Th and U) were determined using a VG Elemental® PQ3 inductively coupled plasma mass spectrometer (ICP-MS) enhanced with a chicane lens system, following the procedures described by Chang *et al.* (2003). Trace element data, except for high-field-strength elements (HFSE: Zr, Nb, Hf and Ta), were obtained after HF–$HClO_4$–HNO_3 digestions. For HFSE analysis, alkali fusion ($LiBO_2$/$Li_2B_4O_7$, Spectroflux® 100B of Johnson Matthey) was applied to ensure a complete decomposition of refractory minor phases. Analytical accuracy and precision for ICP-MS analyses, estimated from repeated measurements of international reference rocks, were better than 10 and 2–5%, respectively.

The analytical procedure used for chemical separation and mass spectrometry for Sr, Nd and Pb isotope determinations was outlined by Yoshikawa *et al.* (2001), Shibata *et al.* (2003) and Miyazaki *et al.* (2003). Total procedural blanks for Sr, Nd and Pb were less than 10, 10 and 5 pg,

Table 1: Compositions of Oto-Zan HMA samples

	SD-249	OTO-1
SiO_2	56·36	58·20
TiO_2	0·62	0·61
Al_2O_3	16·28	16·58
Fe_2O_3*	6·27	6·04
MnO	0·11	0·11
MgO	7·03	6·69
CaO	6·97	6·67
Na_2O	2·99	3·41
K_2O	2·11	1·80
P_2O_5	0·16	0·16
Total	98·90	100·26
$^{87}Sr/^{86}Sr$	0·705567 ± 11	0·705607 ± 11
$(^{87}Sr/^{86}Sr)_i$†	0·70544	0·70548
$^{143}Nd/^{144}Nd$	0·512587 ± 13	0·512590 ± 08
$^{208}Pb/^{204}Pb$	38·620 ± 3	38·645 ± 3
$^{207}Pb/^{204}Pb$	15·600 ± 1	15·607 ± 1
$^{208}Pb/^{204}Pb$	18·378 ± 1	18·385 ± 1

*Total iron as Fe_2O_3; †corrected for 13 Ma.

respectively. Mass spectrometry was performed on a Thermo-Finnigan® Triton TI equipped with nine Faraday cups, using a static multi-collection mode. Normalizing factors used to correct for isotopic fractionation in the Sr, Nd and Pb isotope analyses were $^{86}Sr/^{88}Sr = 0{\cdot}1194$, $^{146}Nd/^{144}Nd = 0{\cdot}7219$, and 0·145 % per atomic mass unit, respectively. Measured isotopic ratios for standard materials were $^{87}Sr/^{86}Sr = 0{\cdot}710268 \pm 19$ (2σ) for NIST 987 ($n = 10$), $^{143}Nd/^{144}Nd = 0{\cdot}511844 \pm 11$ (2σ) for La Jolla ($n = 10$), and $^{208}Pb/^{204}Pb = 36{\cdot}712 \pm 11$ (2σ), $^{207}Pb/^{204}Pb = 15{\cdot}495 \pm 4$ (2σ), $^{206}Pb/^{204}Pb = 16{\cdot}939 \pm 3$ (2σ) for NIST 981 ($n = 35$).

Mineral compositions were analysed using JEOL JXA-8800 and -8900 electron-probe micro-analysers following the method described by Shukuno (2003). The excitation potential, specimen current, and analytical time were: 15 kV, 15 nA and 20 s (25 kV, 20 nA and 100 s for Mn, Ca and Ni analyses) for olivine; 15 kV, 12 nA and 20 s for spinel; 15 kV, 15 nA and 20 s for pyroxene and plagioclase. ZAF correction procedures were employed.

Melting experiments

Starting material

An HMA (SD-249), which forms a part of the Oto-Zan lava flow, was used as the starting material for the experiments (Table 1). This HMA sample possesses a composition almost identical to the sample from the lowermost part of the Oto-Zan lava flow (OTO-1 in Table 1), but with lower Na_2O and higher K_2O contents. Sample SD-249 was selected because it is completely fresh, whereas OTO-1 contains altered glass in the groundmass. In order to adjust the above compositional differences and to apply the experimental results to the Oto-Zan composite lava compositions, we used 'corrected' melt compositions, as described later.

Experimental

Experiments were performed in a Kobelco 500 MPa type internally heated pressure vessel in which pure Ar gas was used as the pressure medium. Three glasses with different water contents were used as starting materials, and were prepared as follows. The powdered sample was first sealed in a Pt capsule (4·7 mm inner diameter, 0·15 mm wall) with a small amount of distilled water. The sample was then heated to 1300–1350°C at 0·2 GPa for 20–30 min, and quenched isobarically. The amounts of H_2O in the recovered glass are 0·7, 1·5 and 2·1 wt %, measured using an FT-IR micro-spectrometer. Although slight Fe-loss occurred (from 5·6 to 5·2–4·9 wt % FeO* from the original sample to the recovered glasses, respectively), no change was observed for other elements.

The glass sample was set in an $Au_{25}Pd$ capsule (2·0 mm inner diameter, 0·15 mm wall), and was hung by Mo wire in the hotspot of a Mo furnace within the pressure vessel and held for 6–75 h at 0·3 GPa and a set temperature. The experimental pressure corresponds to middle-crustal depths beneath the Setouchi volcanic belt. Pressures were measured with a strain-gauge pressure transducer. Temperatures were monitored with two W_5Re–$W_{26}Re$ thermocouples spaced vertically 5 mm apart, and the observed temperature gradient across the sample was less than 10°C. At the end of the run, the hanging wire was cut with a surging current, thereby letting the capsule fall to the cold (<250°C) bottom of the vessel and quench isobarically.

Oxygen fugacity during melting experiments was estimated based on a solution model for coexisting magnetite and ilmenite (Spencer & Lindsley, 1981). Although the observed compositions of magnetite and ilmenite are beyond the upper limit of their oxygen barometer, we tentatively show these estimates in Fig. 2. The experimental device generated redox conditions within a well-defined range at ~NNO+3, which is ~2 log units higher than the oxygen fugacity estimated for the Oto-Zan HMA magma based on olivine–spinel compositions (see below). If this is the case, then the difference in oxygen fugacity will have significant impacts on the stability of oxide minerals and, thereby, could influence the variation of FeO*/MgO and TiO_2 during magmatic differentiation.

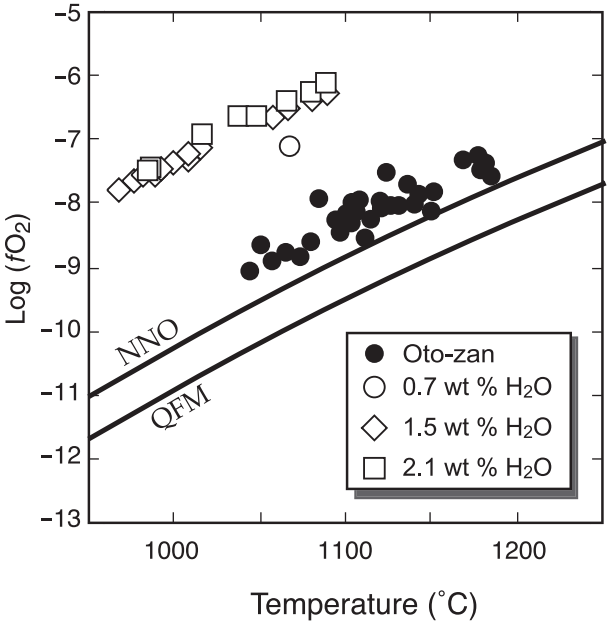

Fig. 2. fO_2 relative to the NNO and QFM oxygen buffers during melting experiments and of the HMA sanukitoid OTO-1 inferred from magnetite–ilmenite compositions (based on method of Spencer & Lindsley, 1981) and spinel compositions based on methods by Ballhaus *et al.* (1990, 1991), and Ballhaus (1993), respectively.

Mineral and glass compositions

Mineral and glass compositions were analysed using JEOL JXA-8800 electron-probe micro-analyser. The excitation potential, specimen current, and analytical time were 15 kv, 12 nA and 20 s, respectively. A defocused electron beam of 10 μm in diameter was used for glass, whereas a focused beam was employed for the measurement of the crystals. ZAF correction procedures were employed.

Modal compositions were calculated by mass balance based on compositions of the starting material, minerals and glasses.

RESULTS

Petrography

Modal proportions of phenocrysts and representative mineral compositions are shown in Tables 2–6. Rocks forming the Oto-Zan lava flow are distinct from typical orogenic andesites in two important ways. First, they are poor in phenocrysts (<15 vol. %). Second, they do not contain plagioclase as a phenocryst phase, which is the major phenocryst phase in typical andesites. These petrographic signatures characterize sanukitoids occurring in the Setouchi volcanic belt. An additional petrographic feature of sanukitoid is its compact nature, i.e. the absence of vesicles.

Table 2: Modal mineralogy of the Oto-Za lava flow as a function of stratigraphic height above the base of the flow

Sample no.	Height (m)	ol	cpx	opx	pl*	qz*	Gm
700	72·0	–	0·6	14·5	0·6	–	84·3
800	71·0	–	0·9	12·4	0·4	0·5	85·7
1200	67·0	–	1·0	12·2	0·5	–	86·3
1400	65·0	–	0·9	11·8	–	–	87·3
1500	64·0	–	0·5	12·4	0·2	–	86·9
1820	60·8	–	0·6	12·4	0·1	–	86·9
1950	59·5	–	1·0	12·5	–	–	86·5
2140	57·6	–	1·4	13·3	–	0·1	85·2
2450	54·5	–	1·5	14·4	0·2	–	83·9
2700	52·0	–	1·0	11·9	–	–	87·1
2860	50·4	–	1·2	12·5	–	–	86·3
2960	49·4	–	1·0	12·3	0·2	–	86·5
3400	45·0	–	1·5	9·8	–	0·1	88·5
3520	43·8	–	1·2	13·1	0·4	–	85·3
3770	41·3	–	1·0	11·5	0·2	0·3	86·8
450-base	39·3	–	1·2	11·7	0·1	–	87·0
350-base	38·3	–	1·3	12·1	0·2	0·1	86·4
100-base	36·3	–	0·8	9·3	–	–	89·9
0-base	34·8	–	0·9	9·7	0·1	–	89·3
OTO-9	29·0	–	0·6	8·7	0·2	–	90·4
802-3	26·3	–	2·9	9·2	–	–	88·0
802-0-2	26·0	0·5	0·2	5·6	0·5	–	93·2
801-8	25·8	3·9	–	5·9	0·3	–	89·9
800-7	24·7	4·5	0·1	3·0	0·3	0·2	91·8
OTO-8	24·0	6·2	0·7	3·6	0·1	0·1	89·1
602-9	21·9	6·7	3·9	1·1	0·3	–	87·8
602-7	21·7	7·8	2·0	0·1	–	–	90·1
602-4	21·4	11·5	0·5	–	0·4	–	87·6
601-5	20·5	9·3	1·7	–	0·7	–	88·3
OTO-7	19·0	6·9	2·7	2·0	0·1	–	88·2
OTO-6·2	16·0	9·3	0·8	–	0·4	–	89·4
OTO-5	12·0	10·5	1·6	–	0·1	–	87·8
OTO-4	6·0	9·4	3·0	–	0·2	–	87·4
OTO-3	3·0	11·2	3·4	–	–	–	85·4
OTO-1	0	9·1	2·9	–	0·2	–	87·7

ol, olivine; cpx, clinopyroxene; opx, orthopyroxene; pl, plagioclase; qz, quartz; gm, groundmass. *Xenocryst.

One petrographic signature observed for the Oto-Zan lava is that both the amount and the assemblage of phenocryst phases change gradually within the single lava flow (Fig. 3), indicating that the lava is a composite flow. The basal part of the lava flow is composed of augite–olivine andesite, with the amount of olivine and augite decreasing upwards. Orthopyroxene, instead of olivine, appears as a phenocryst phase ~20 m from the

Table 3: Representative compositions of olivine phenocrysts

Sample:	OTO-1	OTO-1	OTO-1	OTO-1	OTO-7	OTO-7	OTO-7	OTO-7
Grain:	Ol32	Ol32	Ol38	Ol38	Ol45	Ol45	Ol41B	Ol41B
Position:	core	rim	core	rim	core	rim	core	rim
SiO_2	40·87	40·49	40·61	39·79	40·57	39·73	39·83	39·83
FeO	9·88	11·63	10·92	16·90	12·09	17·95	15·36	17·77
MnO	0·16	0·19	0·18	0·28	0·18	0·30	0·25	0·31
MgO	48·70	47·94	48·15	43·61	48·01	43·34	44·81	43·27
CaO	0·10	0·10	0·10	0·12	0·08	0·08	0·08	0·09
NiO	0·61	0·37	0·48	0·14	0·62	0·25	0·47	0·30
Total	100·34	100·72	100·44	100·86	101·55	101·64	100·80	101·56
Si	1·001	0·995	0·998	0·999	0·992	0·996	0·996	0·998
Fe	0·202	0·239	0·224	0·355	0·247	0·376	0·321	0·372
Mn	0·003	0·004	0·004	0·006	0·004	0·006	0·005	0·007
Mg	1·777	1·756	1·764	1·633	1·750	1·619	1·670	1·617
Ca	0·003	0·003	0·003	0·003	0·002	0·002	0·002	0·002
Ni	0·012	0·007	0·009	0·003	0·012	0·005	0·009	0·006
Total	2·999	3·004	3·002	2·999	3·008	3·004	3·004	3·002
O	4·000	4·000	4·000	4·000	4·000	4·000	4·000	4·000
Mg/(Mg + Fe)	0·898	0·880	0·887	0·821	0·876	0·811	0·839	0·813

base. The upper part of the lava flow comprises augite–orthopyroxene (bronzite to hypersthene) andesite.

Olivine phenocrysts at the base of the lava flow (OTO-1) are more magnesian and characterized by a narrower compositional range than those in the sample at 19 m above the base (OTO-7; Fig. 4). Olivine in OTO-1 has a composition in equilibrium with the bulk rock in terms of Fe–Mg exchange partitioning, whereas that in OTO-7 has Mg-numbers lower than that of inferred equilibrium olivine (Fig. 4). The NiO content at a given Mg-number of olivine phenocryst in OTO-7 is higher than that in OTO-1. The compositional trend for olivine in OTO-1 can be explained by simple olivine fractionation inferred on the basis of Fe–Mg–Ni exchange partitioning between olivine and silicate melts (Roeder & Emslie, 1970; Kinzler *et al.*, 1990) and an assumption of $Fe^{2+}/(Fe^{2+} + Fe^{3+}) = 0{\cdot}9$ in the magma (Fig. 4), whereas some additional processes may be needed for understanding the unusually nickeliferous trend for OTO-7 olivine. Such unusually nickeliferous olivine phenocrysts have been found in some basalts and andesites (e.g. Sato & Banno, 1983; Nabelek & Langmuir, 1986; Nakamura, 1995; Tatsumi *et al.*, 2003, 2004). Nakamura (1995) examined the compositional zoning of olivine phenocrysts in calc-alkalic andesites from the Yatsugatake volcano, Central Japan, by using a growth and diffusion model in the Mg–Fe–Ni system. He showed that the composition of nickeliferous olivine phenocrysts could be explained by diffusion processes within normally zoned olivine, causing Fe-enrichment without a marked depression in the Ni content. This is due to a greater Fe–Mg inter-diffusion coefficient than the Ni tracer-diffusion coefficient in olivine. Tatsumi *et al.* (2003) favored this explanation for the occurrence of unusually nickeliferous olivine in rather olivine-rich (~20 vol. %) sanukitoids (Fig. 4). Although OTO-7 contains only 7 vol. % of olivine phenocrysts, it may be inferred that a long residence time of olivine phenocrysts in the magma may cause such unusual compositions.

Many olivine phenocrysts contain chromite inclusions. In a sample from the base of the lava flow (OTO-1), these spinels show a limited compositional range, whereas those in OTO-7 range from chromite to chromian titanomagnetite (Fig. 5a). The following compositional differences in chromite inclusions should be stressed: (1) chromites in OTO-7 are enriched in Fe^{2+}, Fe^{3+}, Ti and depleted in Mg, Al, Cr compared with those in OTO-1 (Fig. 5a–c); (2) such compositional differences are also observed for chromite included in individual olivine phenocrysts in OTO-7 as a function of the distance from the rim of the olivine crystal. These compositional changes are documented for spinel inclusions in rather phenocryst-rich HMAs from the Setouchi volcanic belt (Fig. 5a–c). Scowen *et al.* (1991) documented similar chemical variability of chromite inclusions in olivine phenocrysts from the 1959 Kilauea Iki lava lake and

Table 4: Representative compositions of spinel inclusions

Sample:	OTO-1	OTO-1	OTO-1	OTO-7	OTO-7	OTO-7
SiO_2	0·08	0·11	0·03	0·07	0·04	0·01
TiO_2	0·43	0·41	0·26	1·08	0·56	0·88
Al_2O_3	14·88	13·47	11·53	6·53	9·37	6·34
Cr_2O_3	50·20	48·82	56·13	27·94	44·58	39·17
FeO	20·65	24·31	20·05	56·41	36·60	44·59
MnO	0·36	0·41	0·31	0·27	0·28	0·28
MgO	13·20	11·13	10·81	3·75	4·71	4·66
Total	99·79	98·65	99·11	96·04	96·14	95·92
Si	0·003	0·004	0·001	0·002	0·002	0·000
Ti	0·010	0·010	0·006	0·029	0·015	0·024
Al	0·554	0·517	0·446	0·276	0·391	0·268
Cr	1·255	1·257	1·458	0·792	1·250	1·111
Fe^{3+}	0·165	0·199	0·081	0·869	0·326	0·573
Fe^{2+}	0·381	0·463	0·469	0·822	0·759	0·765
Mn	0·010	0·011	0·009	0·008	0·008	0·008
Mg	0·622	0·540	0·529	0·200	0·249	0·250
Total	3·000	3·000	3·000	2·999	3·000	3·000
O	4·000	4·000	4·000	4·000	4·000	4·000
Cr/(Cr + Al)	0·694	0·709	0·766	0·742	0·761	0·806
Mg/(Mg + Fe^{2+})	0·620	0·539	0·530	0·196	0·247	0·246
Cr/(Al + Cr + Fe^{3+})	0·636	0·637	0·734	0·409	0·635	0·569
Al/(Al + Cr + Fe^{3+})	0·281	0·262	0·225	0·142	0·199	0·137
Fe^{3+}/(Al + Cr + Fe^{3+})	0·084	0·101	0·041	0·449	0·166	0·293
Olivine[1]	0·893	0·859	0·893	0·778	0·811	0·876

Fe^{3+} and Fe^{3+} are calculated assuming spinel stoichiometry.
[1]Mg/(Mg + Fe) of coexisting olivine.

proposed that the compositional changes may be caused by re-equilibration with the residual melt by cationic diffusion (Mg, Al, Cr outwards and Fe^{2+}, Fe^{3+}, Ti inwards) through the olivine crystals. Re-equilibration of chromite inclusions, but not of the Ni content in the host olivine as described before, implies a significantly larger flux of Al^{3+},Cr^{3+}, Fe^{3+} and Ti^{4+} through the olivine crystal than Ni^{2+}. Although the diffusivities of such elements having high charge have not been measured experimentally, they are likely to be significantly slower than the divalent cations such as Ni. If so, then the explanation for the elevated Ni content in olivine, involving a slow cooling rate, could not be valid for the variability in the composition of chromite. Further work is needed to understand the compositional relationship between chromite inclusions and the host olivine.

Ballhaus *et al.* (1990, 1991) and Ballhaus (1993) examined Cr–Al-rich spinel compositions and demonstrated that Fe^{3+} in spinel may provide a reasonable estimate of the fO_2 relative to the FMQ buffer for a magma. Figure 2 indicates fO_2 estimates based on spinel crystals in the Oto-Zan lava flow and suggests that the fO_2 of the Oto-Zan magma may be close to, or one log-unit higher than, the NNO buffer, which is a typical value for subduction zone magmas (Ballhaus, 1993).

Clinopyroxene phenocrysts in the lower part of the Oto-Zan lava flow are oscillatory zoned and show a wide range in composition (e.g. OTO-1 in Fig. 6). On the other hand, those in olivine-free pyroxene andesites in the upper part of the lava flow (Fig. 3) include both normally zoned and reversely zoned crystals (Table 5). Orthoyroxene-phyric rocks also contain both normally zoned and reversely zoned orthopyroxene phenocrysts (Fig. 6 and Table 6), suggesting some disequilibrium processes operated during magmatic differentiation, such as mixing of magmas with different compositions.

In the middle to upper part of the lava flow, i.e. typically at >20 m above the base and higher, pegmatitic streaks, which consist of cristobalite and minor alkali feldspar and biotite, are developed along platy joints.

Bulk chemical compositions

Major and trace element compositions for all samples, obtained by XRF analysis, are listed in Table 7. Trace element concentrations (ICP-MS) and Sr–Nd–Pb isotopic compositions for representative samples are shown in Tables 8 and 9.

Sanukitoids from the Oto-Zan lava flow exhibit more of a calc-alkalic trend than andesites from Quaternary volcanoes in the NE Japan arc and other sanukitoids in the Setouchi volcanic belt (Fig. 7a). Oto-Zan sanukitoids have N-MORB-normalized incompatible element patterns identical to those in the other regions of the Setouchi volcanic belt (Fig. 7b), which typify both subduction zone magmas and bulk continental crust compositions, i.e. higher concentrations of elements with higher incompatibility during mantle melting and relative depletions and enrichment in Nb–Ta and Pb, respectively. In contrast, boninite, another type of HMA, is more depleted in incompatible trace elements and REEs than sanukitoids (Fig. 7b and c).

The Sr–Nd–Pb isotopic compositions of Oto-Zan sanukitoids are shown in Fig. 8, together with previously reported HMAs and basement rocks from Shodo-Shima Island (Shimoda *et al.*, 1998; Tatsumi *et al.*, 2002). Oto-Zan sanukitoids exhibit more enriched isotopic signatures than other HMAs from the Mito Peninsula (Fig. 1), only ~5 km away from the Oto-Zan.

The compositional variation in the Oto-Zan lava flow as a function of height from the base of the lava flow is shown in Figs 9 and 10. Concentrations of most elements change with increasing height, synchronously with the changes in modal composition (cf. Fig. 3), although the abundance of some elements such as Ba, Pb, Sr, Y and Th, and Nd and Pb isotopic ratios remain essentially

Table 5: Representative compositions of clinopyroxene phenocrysts

Sample:	OTO-1	OTO-1	OTO-1	OTO-1	OTO-7	OTO-7	OTO-7	OTO-7	OTO-9	OTO-9	OTO-9	OTO-9	OTO-9
Grain:	Px30	Px30	Px2	Px2	Px37	Px37	Px22	Px22	Px27	Px27	Px36	Px36	Px36
Position:	core	rim	core	rim	core	rim	core	rim	core	rim	core	mantle	rim
SiO_2	53·39	51·85	52·16	52·52	53·51	53·72	52·01	53·41	55·17	52·90	52·43	52·30	50·75
TiO_2	0·26	0·66	0·52	0·59	0·39	0·37	0·83	0·52	0·25	0·53	0·58	0·34	0·52
Al_2O_3	1·41	3·85	3·15	2·88	2·29	2·39	3·91	2·56	2·27	2·48	3·24	2·99	2·65
Cr_2O_3	0·52	0·51	0·31	0·21	0·40	0·65	0·14	0·24	0·40	0·07	0·04	0·13	0·10
FeO	4·94	5·36	6·26	7·01	4·88	5·97	6·22	6·03	6·98	5·74	7·56	5·77	7·30
MnO	0·17	0·16	0·18	0·27	0·17	0·22	0·20	0·19	0·19	0·12	0·24	0·17	0·22
MgO	18·08	15·62	16·12	16·61	17·09	17·68	16·17	17·16	24·97	16·51	15·31	16·18	15·74
CaO	20·51	21·44	21·24	19·88	20·66	19·37	20·63	20·34	11·34	21·39	20·89	20·97	20·64
Na_2O	0·22	0·28	0·27	0·26	0·24	0·26	0·32	0·27	0·09	0·18	0·19	0·20	0·21
Total	99·49	99·73	100·21	100·23	99·64	100·63	100·42	100·72	101·65	99·92	100·49	99·04	98·13
Si	1·957	1·905	1·914	1·925	1·955	1·947	1·900	1·939	1·940	1·939	1·925	1·933	1·913
Ti	0·007	0·018	0·014	0·016	0·011	0·010	0·023	0·014	0·007	0·014	0·016	0·010	0·015
Al	0·061	0·167	0·136	0·125	0·099	0·102	0·168	0·109	0·094	0·107	0·140	0·130	0·118
Cr	0·015	0·015	0·009	0·006	0·011	0·019	0·004	0·007	0·011	0·002	0·001	0·004	0·003
Fe	0·151	0·165	0·192	0·215	0·149	0·181	0·190	0·183	0·205	0·176	0·232	0·178	0·230
Mn	0·005	0·005	0·006	0·008	0·005	0·007	0·006	0·006	0·006	0·004	0·008	0·005	0·007
Mg	0·988	0·856	0·882	0·908	0·931	0·956	0·881	0·929	1·309	0·903	0·838	0·892	0·884
Ca	0·805	0·844	0·835	0·781	0·809	0·752	0·808	0·791	0·427	0·840	0·822	0·831	0·834
Na	0·016	0·020	0·019	0·019	0·017	0·018	0·022	0·019	0·006	0·013	0·014	0·014	0·015
Total	4·006	3·995	4·009	4·002	3·987	3·991	4·002	3·998	4·004	3·998	3·995	3·997	4·019
O	6·000	6·000	6·000	6·000	6·000	6·000	6·000	6·000	6·000	6·000	6·000	6·000	6·000
Mg/(Mg + Fe)	0·867	0·839	0·821	0·809	0·862	0·841	0·822	0·835	0·864	0·837	0·783	0·833	0·793

constant throughout the lava flow (Figs 9 and 10). Two samples (SD303 at the top and OTO-7 at 19 m from the base) possess higher $^{87}Sr/^{86}Sr$ (>0·7057) than the other samples (~0·7055). This is unlikely to have resulted from selective crustal contamination, because of rather constant $^{143}Nd/^{144}Nd$ compositions for all the samples. An unusual 'spike' in those samples is also documented for Ba (Fig. 9). One possible explanation for such spikes in Sr isotopic composition and Ba abundance may be selective transport of these elements in gas-rich phases that could extensively react with crustal components; there is a higher concentration of Ba and Sr in the pegmatitic streaks that are ubiquitous in the middle to upper part of the lava flow.

Melting phase relations and liquid compositions

The phase assemblages and the average compositions of minerals and glasses are listed in Table 10, and the modal compositions of experimental products in the presence of 0·7, 1·5 and 2·1 wt % H_2O are shown in Fig. 11. In order to apply the melt compositions obtained in the experiments to the Oto-Zan lava compositions, 'corrected' melt compositions were calculated by adjusting the Na_2O and K_2O contents in the starting material (SD-249) to those in the OTO-1 (Tables 1 and 10) and recalculating to 100% total. This should provide reasonable estimates for K_2O and at least for Na_2O in rather high-temperature melts, as these elements are not strongly partitioned into the mineral phases present (e.g. pyroxene; Table 10) and behave largely as incompatible elements.

An important criterion for equilibrium is the achievement of regular and consistent partitioning of major elements between crystalline phases and melt. The calculated orthopyroxene–melt and clinopyroxene–melt Fe–Mg exchange distribution coefficients (K_D^{Fe-Mg}) are 0·24 ± 0·02 (1σ) and 0·31 ± 0·03 (1σ), respectively. The plagioclase–melt Ca–Na exchange distribution coefficient is 2·1 ± 0·2 (1σ). Although the clinopyroxene–melt K_D^{Fe-Mg} is slightly higher, the other exchange distribution coefficients are close to those previously reported (e.g. Gaetani *et al.*, 1993; Sisson & Grove, 1993; Grove *et al.*, 2003). This, together with constant melt and mineral

Table 6: Representative compositions of orthopyroxene phenocrysts

Sample:	OTO-7	OTO-7	OTO-7	OTO-7	OTO-7	OTO-9	OTO-9	OTO-9	OTO-9	OTO-9
Grain:	Px46	Px46	Px44S	Px44S	Px44S	Px9C	Px9C	Px31	Px31	Px32
Position:	core	rim	core	mantle	rim	core	rim	core	mantle	rim
SiO_2	56·84	57·02	53·72	55·73	55·80	57·07	56·37	51·86	56·46	55·69
TiO_2	0·08	0·08	0·08	0·18	0·15	0·12	0·09	0·14	0·07	0·09
Al_2O_3	1·80	0·68	4·19	2·70	1·39	1·51	0·56	5·29	1·53	1·89
Cr_2O_3	0·85	0·31	0·11	0·36	0·37	0·61	0·12	0·03	0·66	0·49
FeO	6·43	11·82	13·28	8·56	10·16	7·71	11·58	18·43	8·02	9·07
MnO	0·15	0·28	0·43	0·16	0·25	0·21	0·29	0·44	0·14	0·25
MgO	32·89	29·50	27·43	30·82	30·39	32·93	29·89	23·10	32·36	30·78
CaO	0·86	1·47	0·87	1·41	1·47	0·87	1·38	1·17	0·86	1·05
Na_2O	0·04	0·01	0·01	0·02	0·04	0·03	0·03	0·05	0·01	0·03
Total	99·92	101·17	100·13	99·94	100·03	101·06	100·30	100·51	100·11	99·35
Si	1·966	1·996	1·914	1·948	1·965	1·964	1·990	1·888	1·964	1·962
Ti	0·002	0·002	0·002	0·005	0·004	0·003	0·002	0·004	0·002	0·002
Al	0·073	0·028	0·176	0·111	0·058	0·061	0·023	0·227	0·063	0·078
Cr	0·023	0·009	0·003	0·010	0·010	0·017	0·003	0·001	0·018	0·014
Fe	0·186	0·346	0·396	0·250	0·299	0·222	0·342	0·561	0·233	0·267
Mn	0·004	0·008	0·013	0·005	0·007	0·006	0·009	0·014	0·004	0·007
Mg	1·696	1·539	1·457	1·605	1·596	1·689	1·573	1·253	1·678	1·617
Ca	0·032	0·055	0·033	0·053	0·056	0·032	0·052	0·046	0·032	0·040
Na	0·002	0·000	0·001	0·001	0·003	0·002	0·002	0·003	0·001	0·002
Total	3·985	3·984	3·995	3·988	3·998	3·996	3·996	3·996	3·994	3·990
O	6·000	6·000	6·000	6·000	6·000	6·000	6·000	6·000	6·000	6·000
Mg/(Mg + Fe)	0·901	0·816	0·786	0·865	0·842	0·884	0·822	0·691	0·878	0·858

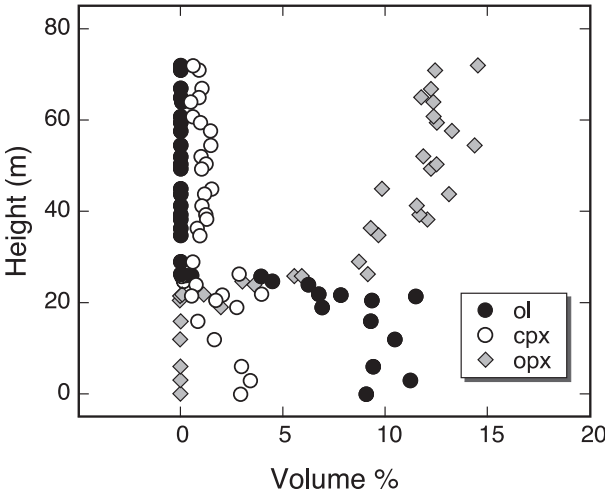

Fig. 3. Variation of modal minerology throughout the Oto-Zan lava flow as a function of height above the base. The phenocryst assemblage changes from olivine (ol) + clinopyroxene (cpx) in the basal part, via olivine + clinopyroxene + orthopyroxene (opx), to orthopyroxene + clinopyroxene in the upper part of the lava flow, indicating that the Oto-Zan lava forms a composite lava flow. The absence of plagioclase phenocrysts, which characterizes sanukitoids in the Setouchi volcanic belt, is significant.

compositions within each run product (Table 10), suggests a sufficiently close approach to equilibrium.

The 'corrected' melt compositions are plotted in Fig. 12, together with the compositional range of the Oto-Zan composite lava flow. In the FeO*/MgO vs SiO_2 diagram, the liquid line of descent obtained for the Oto-Zan HMA is close to that for an HMA from the Mt Shasta region (Grove *et al.*, 2002). In a strict sense, this crystallization path, especially in its early stage, does not follow a calc-alkalic differentiation trend because the degree of increasing FeO*/MgO against SiO_2 content is greater than that defined by Miyashiro (1974). It should be stressed that differences in the H_2O content of the starting materials (0·7, 1·5 and 2·1 wt %) do not yield significant changes in the liquid line of descent, although small but systematic differences are recognized for TiO_2 and Al_2O_3 (Fig. 12).

The experimental product after a run at 900°C in the presence of 0·7 wt % H_2O contains only a small amount of glass, suggesting that this temperature is close to the solidus (Fig. 11). At this temperature, amphibole and biotite are also observed in the run products, suggesting that the subsolidus mineral assemblage includes

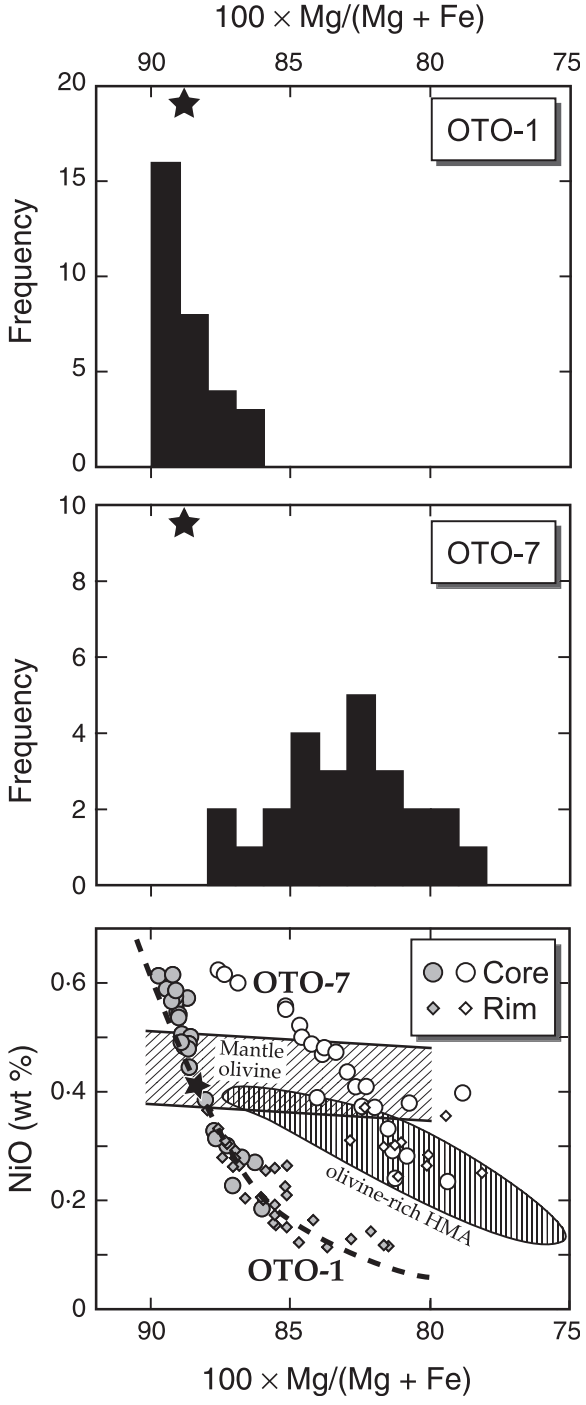

Fig. 4. Compositions of olivine phenocrysts in two samples (OTO-1, OTO-7) from the Oto-Zan composite lava flow. Stars indicate compositions of olivine in equilibrium with the host rock, calculated based on Fe–Mg–Ni exchange partitioning and an inferred Fe^{3+}/Fe^{2+} ratio in the magma. An olivine perfect fractionation trend is also shown by the dashed line (see text). Olivine phenocrysts in OTO-7, as well as those in olivine-rich HMAs from other regions of the Setouchi volcanic belt, have compositions in disequilibrium with the magma. Compositional ranges of olivine in mantle peridotites (Sato, 1977; Takahashi, 1990) and olivine-rich Setouchi HMAs (Tatsumi *et al.*, 2003) are shown.

amphibole and biotite in addition to plagioclase, Fe–Ti oxide and pyroxene. Although the modal abundance of these phases could not be determined from the present experiments, the total amount of H_2O held in the subsolidus phases can be constrained to less than 1 wt %. It is worth pointing out that even if the subsolidus modal assemblage were 100% hornblende, it would still only contain ~2 wt % H_2O. As the experimental starting material has a composition consistent with a mantle-derived HMA that originally contains ~7 wt % H_2O (Tatsumi, 1982), this result indicates that H_2O can be effectively extracted from a mantle-derived hydrous HMA magma through solidification.

DISCUSSION

The reasons for interest in the origin of the Oto-Zan composite lava flow are twofold. First, there is a paradox concerning the origin of Setouchi HMA magmas; andesites forming the composite lava flows are poor in both phenocrysts and H_2O, although the HMA compositions found at the base of the lava flows may have originally contained a large amount of H_2O during their final equilibration in the uppermost mantle. Second, HMAs in the Setouchi volcanic belt often form composite lava flows and dykes, suggesting that some particular processes may have contributed to the formation of Setouchi HMAs.

Mantle-derived hydrous HMA magma

HMA at the base of the Oto-Zan lava flow

Andesites comprising the Oto-Zan lava flow possess FeO*/MgO ratios smaller than unity (Fig. 7a and Table 7) and are referred to as HMA magmas. In particular, those forming the basal part of the lava flow (e.g. OTO-1) contain Mg-rich olivine (up to Mg-number of 90) and Cr-rich chromite ($Cr/(Cr + Al + Fe^{3+}) > 0{\cdot}7$; Figs 4 and 5, and Tables 3 and 4), which typify HMAs in the Setouchi volcanic belt and other subduction zones (e.g. Tatsumi & Ishizaka, 1981, 1982*a*, 1982*b*). However, the relationship between Mg-number and NiO content in olivine from OTO-1 (Fig. 4) suggests that this HMA is differentiated, as the olivine that is in equilibrium with the bulk OTO-1 is less nickeliferous and less magnesian than the most Ni- and Mg-rich olivine phenocrysts in the sample.

Two HMAs (TGI from the Osaka region of the Setouchi volcanic belt and SD-261 on Shodo-Shima Island; Table 7) have been proposed as least-differentiated, near primary andesite magmas that were produced in the upper mantle leaving harzburgitic and lherzolitic residues, respectively, based on both petrographic examination and melting phase relations at high pressures (Tatsumi, 1981, 1982; Tatsumi &

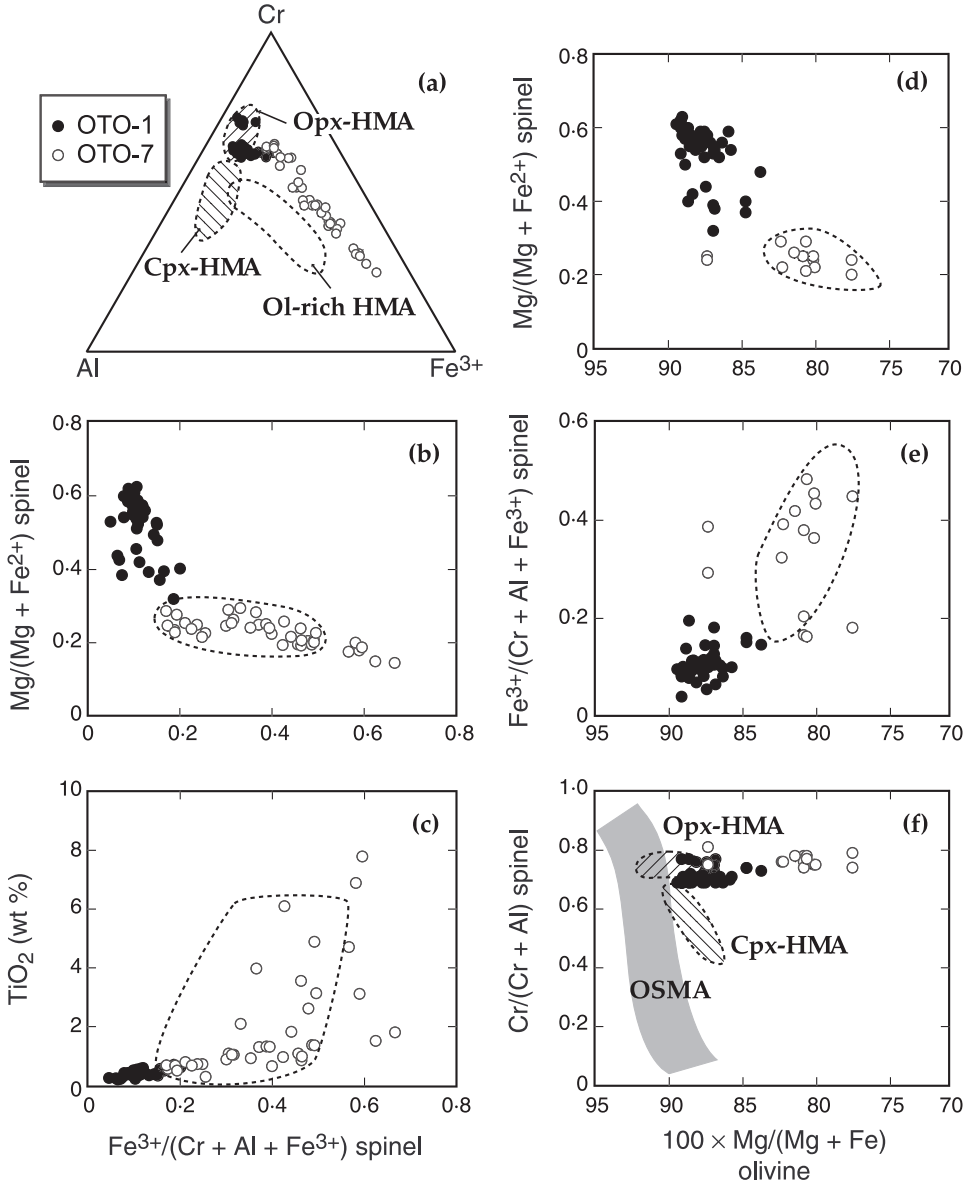

Fig. 5. Compositions of chromite inclusions in olivine phenocrysts (a, b and c) and spinel–olivine compositional relations (d, e and f) in sanukitoids from the Oto-Zan composite lava flow and other regions in the Setouchi volcanic belt. The unusual Fe^{3+}-rich compositional trend for chromites in OTO-7, as well as those characteristically observed for olivine-rich HMA sanukitoids, can be explained by elemental diffusion through the olivine crystals associated with the long residence time and slow rate of cooling of the magmas (see text). Data for HMAs are from Tatsumi & Ishizaka (1981, 1982*a*, 1982*b*) and Tatsumi *et al.* (2003). OSMA, olivine spinel mantle array (Arai, 1994).

Ishizaka, 1981, 1982*a*, 1982*b*). Although the composition of the HMA OTO-1 may be modified a little by olivine fractionation, as mentioned above, the compositional similarity between those HMAs and OTO-1 suggests that the parental magma for the Oto-Zan lava flow was andesitic and possessed a composition close to the OTO-1 HMA. Furthermore, the Oto-Zan HMAs have incompatible trace element and REE characteristics identical to those of HMAs in other regions of the Setouchi volcanic belt (Fig. 7b and c), providing compelling evidence that the Oto-Zan HMA magma was produced in the upper mantle.

Although experimental results indicate that Setouchi HMA magmas can equilibrate with mantle peridotites solely under hydrous conditions, this does not necessarily require the direct addition of slab-derived aqueous fluids to the mantle wedge. Many researchers (e.g. Pearce *et al.*, 1992; Yogodzinski *et al.*, 1994; Kelemen, 1995) have

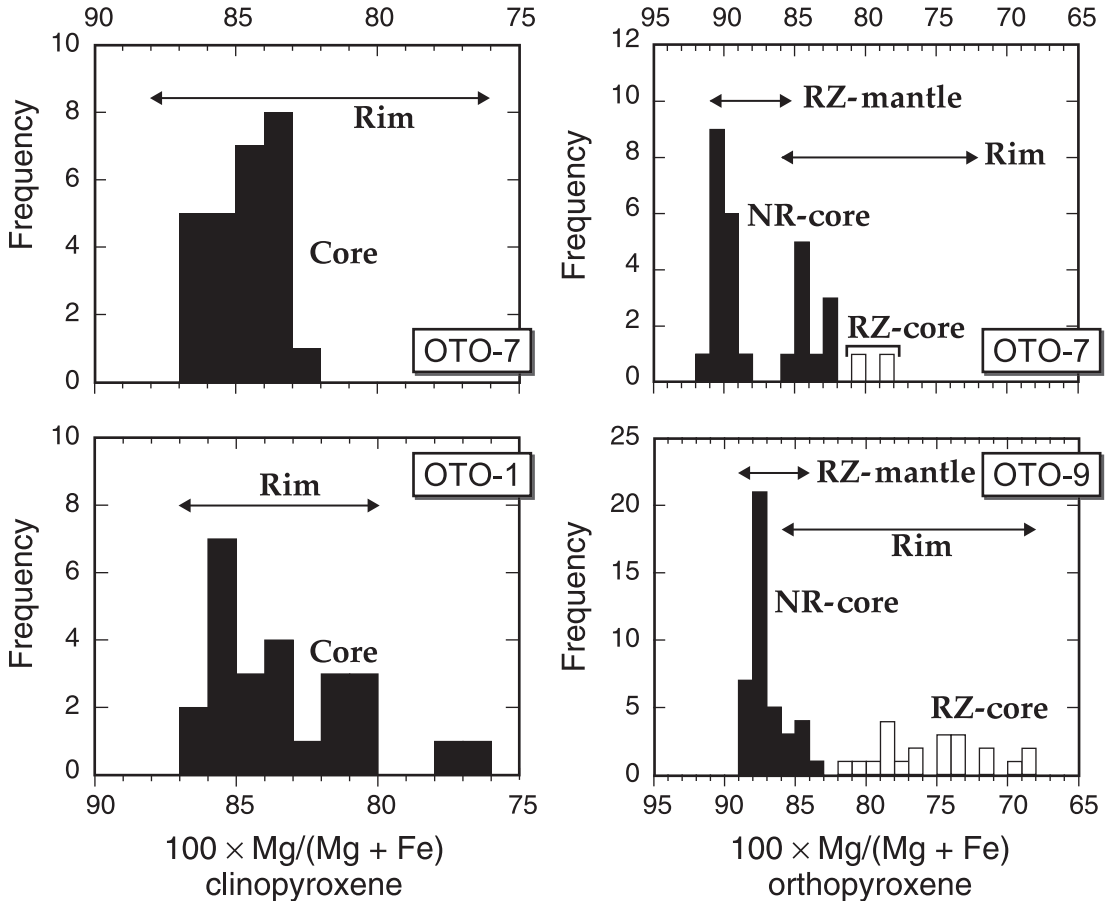

Fig. 6. Compositions of pyroxene phenocrysts in three samples from the Oto-Zan composite lava flow. Both reversely zoned (RZ) and normally zoned (NR) orthopyroxene phenocrysts are observed in Oto-Zan sanukitoids, suggesting mixing of compositionally different magmas during magmatic differentiation processes.

favoured a mechanism for HMA magma production that involves partial melting of the subducting lithosphere and interaction of these slab-derived, hydrous, silicic melts with the overlying mantle wedge peridotite, as originally proposed by Kay (1978). The geochemical characteristics of Setouchi HMAs can be quantitatively explained by this mechanism (Tatsumi, 2001; Hanyu *et al.*, 2002; Tatsumi & Hanyu, 2003).

If such a mechanism was the case for generation of Oto-Zan and other Setouchi HMA magmas, then the Oto-Zan HMA magma must have contained a large amount of H_2O when it was in final equilibrium with mantle peridotite. Experimental results for Setouchi HMAs under H_2O-undersaturated conditions (Tatsumi, 1981, 1982) suggest that ~7 wt % H_2O in the magma is needed for equilibration at 1·0 GPa—a pressure equivalent to the depth immediately below the Moho beneath the Setouchi volcanic belt. It should be stressed, however, that the Oto-Zan HMA, as well as other Setouchi HMAs, contain little H_2O as supported by the present XRF data (Table 7); a HMA from the Oto-Zan lava flow (SD-249) contains 0·89 wt % H_2O(+) (Tatsumi & Ishizaka, 1982*a*), much smaller than boninites (2–5 wt %; Dobson & O'Neil, 1987; Sobolev & Danyushevsky, 1994). Boninites are also distinct from Setouchi HMAs in containing much larger amounts of phenocrysts, up to ~40% (e.g. Umino & Kushiro, 1989), which is consistent with extensive crystallization caused by H_2O-oversaturation during magmatic ascent. It may, thus, be suggested that some particular processes may operate for producing phenocryst-poor and H_2O-poor Setouchi HMAs that are originally rich in H_2O and must become saturated with H_2O within the crust.

Source heterogeneity

The Sr–Nd–Pb isotopic compositions of the Oto-Zan lava samples are clearly different from those of other HMAs from Mito Peninsula on Shodo-Shima island (Figs 1 and 8). This is also the case for Hf isotopes (Hanyu *et al.*, 2002); an Oto-Zan HMA sample (SD-

Table 7: Major and trace element compositions measured by XRF of the Oto-Zan lava flow

	Oto-Zan Lava																
Sample:	SD-303	TOP	280E	380E	430E	500E	540E	620E	700E	700	760	800	1200	1300	1400	1500	1570
Height (m):	80·0	79·0	76·2	75·2	74·7	74·0	73·6	72·8	72·0	72·0	71·4	71·0	67·0	66·0	65·0	64·0	63·3
SiO_2	62·03	61·79	62·04	61·81	62·09	62·01	62·24	62·37	62·22	62·43	62·29	62·31	62·16	62·21	62·39	62·08	62·37
TiO_2	0·52	0·53	0·53	0·53	0·54	0·53	0·54	0·53	0·53	0·53	0·53	0·53	0·53	0·53	0·53	0·53	0·53
Al_2O_3	16·45	16·54	16·58	16·48	16·69	16·67	16·69	16·55	16·71	16·87	16·57	16·71	16·66	16·51	16·52	16·76	16·57
Fe_2O_3*	4·78	4·84	4·87	4·81	4·92	4·84	4·83	4·82	4·87	4·97	4·89	4·80	4·88	4·87	4·83	4·83	4·89
MnO	0·08	0·08	0·08	0·08	0·09	0·08	0·11	0·08	0·08	0·07	0·08	0·07	0·08	0·08	0·08	0·07	0·08
MgO	4·71	5·07	5·07	5·01	5·08	4·85	4·90	5·06	5·12	4·79	5·05	4·54	4·98	5·18	4·99	4·57	4·99
CaO	4·70	5·07	5·00	5·04	5·00	4·98	5·08	5·01	5·03	4·50	4·84	4·77	4·80	4·94	4·86	4·72	4·85
Na_2O	3·81	3·80	3·74	3·77	3·80	3·79	3·81	3·79	3·80	3·67	3·73	3·74	3·77	3·78	3·85	3·78	3·80
K_2O	2·15	1·97	1·96	1·97	1·95	1·97	1·96	1·96	1·97	2·00	1·98	1·98	1·98	2·00	2·00	1·98	1·97
P_2O_5	0·15	0·16	0·16	0·15	0·15	0·17	0·15	0·15	0·15	0·15	0·15	0·16	0·15	0·16	0·16	0·15	0·15
Total	99·38	99·86	100·03	99·66	100·31	99·88	100·29	100·32	100·48	99·99	100·12	99·61	99·99	100·25	100·19	99·46	100·18
FeO*/MgO	0·913	0·859	0·864	0·864	0·873	0·898	0·888	0·858	0·856	0·935	0·872	0·951	0·880	0·845	0·870	0·952	0·881
Ba	304	311	327	351	368	626	325	595	315	480	355	577	405	314	319	426	381
Ni	109	135	123	121	131	127	129	129	132	114	108	111	112	115	111	103	112
Cu	29	22	31	26	24	30	27	23	23	24	25	23	21	21	27	25	26
Zn	62	64	60	70	76	72	63	66	60	59	63	61	60	71	66	58	66
Pb	22	21	20	22	28	26	23	20	19	25	23	25	21	30	29	22	22
Th	7	7	7	8	7	7	7	7	8	7	7	7	7	7	7	8	7
Rb	84	82	81	80	81	81	80	81	81	83	82	82	82	82	82	82	83
Sr	306	323	321	327	322	336	320	333	323	340	323	370	330	319	321	341	318
Y	13	16	14	15	14	14	15	15	13	13	13	17	13	13	13	14	13
Zr	132	129	129	130	127	128	129	128	129	129	127	128	128	125	129	128	127
Nb	6	6	5	6	5	5	6	5	6	6	6	6	6	6	6	6	6

	1610	1820	1950	2050	2140	2450	2660	2700	2790	2860	2960	3400	3520	3690	3720	3750	3770	450base
	62·9	60·8	59·5	58·5	57·6	54·5	52·4	52·0	51·1	50·4	49·4	45·0	43·8	42·1	41·8	41·5	41·3	39·3
SiO_2	62·49	61·97	62·36	62·49	62·19	62·14	62·39	62·13	62·03	62·06	62·07	62·28	61·70	61·91	61·90	62·09	62·13	61·89
TiO_2	0·52	0·53	0·53	0·53	0·53	0·53	0·53	0·53	0·53	0·53	0·53	0·53	0·53	0·53	0·53	0·54	0·53	0·53
Al_2O_3	16·49	16·53	16·67	16·62	16·72	16·54	16·67	16·56	16·49	16·57	16·54	16·60	16·69	16·55	16·61	16·62	16·64	16·48
Fe_2O_3*	4·81	4·87	4·84	4·88	4·86	4·84	4·92	4·83	4·93	4·89	4·90	4·94	4·95	4·88	4·95	4·89	4·98	4·82
MnO	0·08	0·09	0·08	0·09	0·08	0·08	0·08	0·09	0·10	0·09	0·11	0·09	0·09	0·08	0·10	0·08	0·09	0·08
MgO	5·12	5·25	4·99	5·13	4·80	5·06	5·03	5·22	5·12	5·11	5·17	5·12	5·21	5·14	4·92	5·04	5·04	4·97
CaO	4·90	4·98	4·82	4·99	4·80	4·94	4·93	5·05	4·98	4·94	5·04	5·08	4·75	5·07	4·99	4·88	4·96	4·86
Na_2O	3·83	3·83	3·75	3·88	3·81	3·80	3·75	3·89	3·74	3·80	3·78	3·85	3·70	3·78	3·79	3·78	3·75	3·78
K_2O	1·98	1·99	1·99	1·98	1·99	1·99	1·98	2·01	1·96	1·99	1·99	1·97	1·98	1·94	1·97	2·00	1·98	1·98
P_2O_5	0·15	0·15	0·17	0·15	0·15	0·15	0·15	0·16	0·16	0·15	0·15	0·16	0·15	0·15	0·15	0·16	0·16	0·15
Total	100·37	100·18	100·20	100·74	99·93	100·07	100·43	100·45	100·02	100·13	100·26	100·61	99·75	100·03	99·90	100·07	100·26	99·52
FeO*/MgO	0·847	0·835	0·873	0·855	0·910	0·861	0·881	0·833	0·867	0·860	0·852	0·867	0·854	0·855	0·905	0·873	0·888	0·872
Ba	326	312	317	342	329	323	332	327	349	317	323	310	313	338	321	322	335	417
Ni	111	122	105	110	102	122	114	116	116	118	122	114	122	117	121	110	108	110
Cu	25	27	18	27	25	29	22	28	22	24	23	21	30	26	23	24	23	76
Zn	64	60	66	65	57	59	62	60	63	57	62	58	62	61	64	61	58	57

Table 7: continued

	1610	1820	1950	2050	2140	2450	2660	2700	2790	2860	2960	3400	3520	3690	3720	3750	3770	450base
Pb	31	24	22	24	22	23	20	24	22	19	22	21	26	22	24	21	23	22
Th	6	7	7	7	6	8	7	6	7	7	7	8	7	7	7	7	7	8
Rb	81	81	83	82	82	82	82	82	80	83	82	81	81	80	81	85	82	83
Sr	348	320	325	322	323	330	315	320	320	314	318	318	308	321	315	310	315	332
Y	13	14	13	13	12	14	17	13	15	13	14	13	13	14	15	13	13	13
Zr	124	126	127	126	127	126	128	126	125	126	126	125	126	125	127	127	126	126
Nb	5	6	6	6	6	6	6	6	6	6	6	5	6	6	6	6	6	6

	350base	100base	50base	0base	OTO-10	OTO-9	802-3	802-0-2	802-0	801-8	801-4	801-0	800-7	800-4	OTO-8	800-0	700-7	700-5
	38·3	36·3	35·3	34·8	34·0	29·0	26·3	26·0	26·0	25·8	25·4	25·0	24·7	24·4	24·0	24·0	23·7	23·5
SiO_2	62·37	62·27	62·20	62·35	62·86	62·49	60·62	61·79	61·98	61·94	59·93	59·70	59·91	60·36	61·85	60·35	59·42	59·44
TiO_2	0·53	0·52	0·53	0·53	0·53	0·55	0·53	0·53	0·52	0·53	0·53	0·56	0·52	0·53	0·53	0·56	0·58	0·58
Al_2O_3	16·71	16·54	16·62	16·61	16·43	16·74	16·27	16·64	16·59	16·46	16·10	15·98	15·93	16·15	16·42	16·21	15·95	16·05
Fe_2O_3*	4·85	4·82	4·90	4·88	4·75	4·92	4·96	4·74	4·67	4·77	4·84	5·06	4·78	4·82	4·90	5·16	5·43	5·36
MnO	0·08	0·08	0·08	0·08	0·09	0·08	0·09	0·07	0·07	0·08	0·08	0·09	0·08	0·09	0·09	0·09	0·09	0·09
MgO	4·92	5·10	5·17	4·77	4·96	4·47	5·04	4·76	4·78	4·90	5·22	5·61	5·13	5·25	5·29	5·54	6·09	6·08
CaO	4·74	4·82	4·87	4·90	4·64	4·95	5·03	4·90	4·88	5·00	4·99	5·36	4·94	5·04	5·06	5·36	5·68	5·70
Na_2O	3·78	3·77	3·78	3·83	3·78	3·89	3·80	3·82	3·82	3·80	3·77	3·68	3·74	3·74	3·78	3·67	3·58	3·54
K_2O	1·98	1·98	1·99	1·98	2·05	1·92	1·98	1·95	1·97	1·92	1·97	1·86	1·93	1·96	1·98	1·88	1·82	1·83
P_2O_5	0·16	0·15	0·16	0·16	0·15	0·16	0·15	0·16	0·16	0·16	0·15	0·16	0·15	0·16	0·15	0·15	0·15	0·15
Total	100·10	100·06	100·31	100·08	100·23	100·16	98·46	99·36	99·43	99·55	97·57	98·04	97·12	98·10	100·06	98·96	98·78	98·81
FeO*/MgO	0·887	0·852	0·853	0·920	0·861	0·989	0·885	0·896	0·880	0·877	0·833	0·812	0·838	0·827	0·833	0·838	0·802	0·793
Ba	338	317	322	313	328	315	319	320	353	302	304	343	301	304	310	312	669	568
Ni	112	116	118	103	114	91	123	111	108	126	133	150	135	142	134	146	173	171
Cu	8	9	14	20	25	20	24	25	23	21	21	18	23	22	21	22	34	37
Zn	55	57	65	56	63	61	62	72	61	65	60	64	74	61	65	66	66	70
Pb	20	20	23	19	22	21	21	26	24	22	22	23	24	21	23	22	22	25
Th	7	7	6	7	8	7	7	7	7	7	7	6	8	7	8	7	6	6
Rb	82	83	83	83	87	77	82	81	82	80	81	77	81	81	82	78	76	76
Sr	314	312	315	317	304	301	313	312	316	315	316	323	320	323	319	319	334	320
Y	12	13	13	14	15	14	12	13	13	14	12	13	14	14	14	14	13	13
Zr	126	125	127	126	130	135	123	126	125	126	123	118	126	126	125	120	112	113
Nb	6	6	6	6	5	6	6	5	5	5	5	5	5	6	5	5	5	6

	700-1B	700-1A	603-3	603-1	602-9	602-7	602-4	602-2	602-0-2	602-0-1	601-8	601-7	601-5	601-4	601-3	601-2	601-1	601-0
	23·0	23·0	22·3	22·1	21·9	21·7	21·4	21·2	21·0	21·0	20·8	20·7	20·5	20·4	20·3	20·2	20·1	20·0
SiO_2	59·67	59·51	59·50	59·21	59·67	59·17	59·34	60·02	59·16	59·49	58·83	58·91	59·03	59·21	59·28	58·78	58·69	58·83
TiO_2	0·58	0·58	0·58	0·58	0·58	0·57	0·58	0·58	0·58	0·58	0·58	0·59	0·58	0·59	0·59	0·59	0·59	0·59
Al_2O_3	16·04	16·04	15·88	16·13	16·02	15·87	16·14	16·16	16·04	16·15	16·09	16·28	16·15	16·21	16·30	16·10	16·28	16·30
Fe_2O_3*	5·37	5·43	5·45	5·38	5·29	5·32	5·38	5·21	5·56	5·44	5·68	5·55	5·56	5·61	5·55	5·51	5·68	5·65
MnO	0·10	0·10	0·13	0·13	0·13	0·11	0·09	0·12	0·13	0·12	0·10	0·11	0·11	0·12	0·12	0·10	0·09	0·12
MgO	6·30	6·18	6·65	6·32	6·28	6·19	6·18	5·74	6·13	6·04	6·31	6·21	6·41	6·27	6·15	5·96	6·10	6·27
CaO	5·68	5·57	5·78	5·67	5·75	5·61	5·74	5·70	5·73	5·73	5·91	6·12	6·00	6·00	6·10	6·00	6·11	6·15
Na_2O	3·66	3·64	3·58	3·56	3·56	3·58	3·59	3·55	3·54	3·61	3·51	3·52	3·51	3·51	3·57	3·47	3·47	3·49
K_2O	1·81	1·81	1·81	1·85	1·84	1·81	1·79	1·81	1·78	1·80	1·79	1·78	1·78	1·77	1·78	1·78	1·77	1·77

	700-1B	700-1A	603-3	603-1	602-9	602-7	602-4	602-2	602-0-2	602-0-1	601-8	601-7	601-5	601-4	601-3	601-2	601-1	601-0
P_2O_5	0·16	0·16	0·15	0·15	0·15	0·16	0·16	0·16	0·16	0·16	0·16	0·16	0·16	0·16	0·16	0·16	0·16	0·16
Total	99·37	99·02	99·50	98·97	99·26	98·39	99·00	99·04	98·80	99·12	98·96	99·23	99·27	99·46	99·61	98·45	98·95	99·33
FeO*/MgO	0·768	0·792	0·738	0·765	0·758	0·774	0·784	0·817	0·816	0·811	0·810	0·805	0·781	0·805	0·811	0·832	0·839	0·810
Ba	298	328	322	355	362	348	334	563	313	345	301	320	317	338	328	327	322	337
Ni	194	163	201	171	173	190	179	178	176	163	177	177	189	173	179	171	166	174
Cu	34	32	34	34	34	32	32	29	36	31	29	34	35	35	32	34	36	33
Zn	63	63	61	69	64	62	64	63	62	63	65	60	61	65	62	61	62	65
Pb	20	20	21	22	20	20	22	20	20	20	21	21	20	20	19	20	20	19
Th	7	6	7	6	6	6	6	6	6	6	7	6	6	6	6	6	6	7
Rb	75	75	75	76	76	75	74	74	74	74	73	72	72	72	71	73	72	72
Sr	310	310	318	319	315	314	314	322	312	312	314	318	314	315	318	315	314	313
Y	14	13	14	14	14	15	14	15	13	14	13	14	13	14	14	14	14	14
Zr	117	119	112	114	126	116	118	119	118	118	117	117	117	116	115	116	115	113
Nb	6	6	5	5	6	6	6	6	6	6	6	6	6	6	6	6	6	6

																	Setouchi HMA	
	600-9	600-7	600-5	600-1	OTO-7	600-0	500-53	500-46	500-44	500-32	OTO-6·2	500-21	OTO-5	OTO-4	OTO-3	OTO-1	TGI	SD-261
	19·9	19·7	19·5	19·1	19·0	19·0	18·3	17·6	17·4	16·2	16·0	15·1	12·0	6·0	3·0	0		
SiO_2	58·73	59·13	58·55	58·84	60·37	58·68	58·77	58·99	58·68	57·90	59·30	58·33	58·47	58·44	58·47	58·20	57·27	55·37
TiO_2	0·60	0·59	0·59	0·59	0·58	0·59	0·59	0·60	0·59	0·61	0·59	0·60	0·60	0·60	0·60	0·61	0·42	0·65
Al_2O_3	16·39	16·36	16·17	16·26	16·20	16·33	16·22	16·33	16·32	16·56	16·33	16·39	16·50	16·43	16·63	16·58	14·26	15·55
Fe_2O_3*	5·62	5·44	5·66	5·63	5·42	5·57	5·67	5·67	5·65	6·00	5·72	5·90	5·91	5·95	6·05	6·04	6·19	6·23
MnO	0·10	0·10	0·10	0·10	0·10	0·14	0·11	0·10	0·10	0·11	0·10	0·11	0·10	0·10	0·11	0·11	0·12	0·17
MgO	6·05	6·09	6·34	6·16	6·58	6·29	6·37	6·24	6·25	6·37	6·53	6·23	6·62	6·55	6·45	6·69	9·46	6·89
CaO	6·17	6·20	6·15	6·16	5·68	6·21	6·16	6·20	6·26	6·53	6·15	6·55	6·63	6·52	6·63	6·67	6·31	7·04
Na_2O	3·48	3·50	3·44	3·53	3·63	3·49	3·49	3·50	3·46	3·43	3·52	3·40	3·41	3·38	3·46	3·41	2·57	2·84
K_2O	1·78	1·77	1·75	1·75	1·82	1·77	1·76	1·76	1·73	1·76	1·77	1·73	1·75	1·75	1·77	1·80	1·16	2·25
P_2O_5	0·16	0·16	0·16	0·16	0·16	0·16	0·16	0·16	0·16	0·16	0·16	0·16	0·16	0·15	0·16	0·16	0·10	0·17
Total	99·08	99·33	98·89	99·16	100·54	99·23	99·28	99·55	99·20	99·41	100·16	99·39	100·16	99·85	100·33	100·26	97·86	97·16
FeO*/MgO	0·836	0·803	0·804	0·822	0·742	0·798	0·800	0·818	0·815	0·849	0·788	0·852	0·804	0·818	0·844	0·813	0·654	0·814
Ba	331	335	324	317	283	366	356	364	379	394	308	376	296	287	289	277	336	195
Ni	165	172	172	176	180	169	181	174	169	155	181	147	170	190	174	158	179	148
Cu	33	31	30	30	31	33	28	29	28	30	35	25	32	33	37	37		
Zn	65	61	62	64	60	66	64	66	66	68	63	67	61	63	63	63		
Pb	20	19	19	19	21	18	20	21	20	18	21	19	19	20	19	19	13	17
Th	5	6	6	6	6	6	5	6	6	6	6	6	6	5	6	6	5	5
Rb	72	72	71	71	74	72	71	71	71	70	71	70	69	68	68	68	45	114
Sr	316	319	313	314	306	311	313	314	314	317	315	327	314	314	319	316	308	267
Y	13	14	14	14	13	14	14	14	14	14	14	14	14	14	14	13	11	15
Zr	114	114	112	112	116	115	111	112	111	106	115	107	106	104	105	107	94	80
Nb	6	6	6	6	5	6	6	6	5	5	6	5	5	5	5	5	3	5

Fe_2O_3*, total iron as Fe_2O_3; FeO*, total iron as FeO.

249) possesses an ε_{Hf} of 6·5, significantly lower than other Shodo-Shima HMAs (7·6–8·9). One possible explanation for the difference in isotopic composition, especially in terms of Sr–Nd isotopes, would be contamination by crustal materials, as basement rocks, including granite, gneiss and gabbro, have much higher $^{87}Sr/^{86}Sr$ and lower $^{143}Nd/^{144}Nd$ than the HMAs (Fig. 8). The presence of xenocrystic minerals such as quartz and Na-rich

Table 8: Trace element concentrations by ICP-MS

Sample:	OTO-1	OTO-3	OTO-4	OTO-5	OTO-7	OTO-9
Height (m):	0	3·0	6·0	12·0	19·0	29·0
Sc	17·9	18·0	17·9	18·5	15·8	13·2
Rb	71·8	72·5	70·4	74·6	80·1	81·3
Sr	299	298	287	301	293	284
Y	15·0	15·7	15·9	14·7	14·7	16·1
Zr	105	102	103	103	111	135
Nb	5·01	5·04	5·18	5·11	5·59	6·13
Ba	289	307	298	317	312	345
Cs	6·99	5·29	5·61	6·31	4·48	3·07
La	13·9	14·2	14·1	13·6	15·3	18·2
Ce	29·4	28·5	28·4	28·7	31·5	35·2
Pr	3·26	3·26	3·24	3·24	3·48	4·21
Nd	12·6	12·9	12·7	12·6	13·5	15·9
Sm	2·60	2·78	2·70	2·66	2·81	3·26
Eu	0·815	0·846	0·827	0·816	0·838	0·930
Gd	2·55	2·60	2·57	2·50	2·61	2·86
Tb	0·402	0·405	0·398	0·392	0·392	0·440
Dy	2·44	2·49	2·46	2·39	2·41	2·63
Ho	0·495	0·513	0·501	0·485	0·486	0·524
Er	1·45	1·50	1·47	1·41	1·41	1·52
Tm	0·215	0·213	0·214	0·207	0·201	0·216
Yb	1·38	1·43	1·41	1·39	1·35	1·49
Lu	0·212	0·215	0·215	0·209	0·205	0·226
Hf	2·94	2·87	2·92	2·85	3·18	3·53
Ta	0·412	0·416	0·435	0·413	0·485	0·520
Tl	0·384	0·310	0·384	0·331	0·364	0·281
Pb	18·8	18·3	20·3	19·2	20·0	19·7
Th	5·49	5·42	5·39	5·38	5·84	6·23
U	2·17	2·09	2·08	2·11	2·37	2·43

plagioclase in the Oto-Zan lava flow (Table 2) may be consistent with this mechanism. However, Pb isotopic compositions for the Shodo-Shima basement rocks do not support the involvement of crustal materials in the magmatic differentiation of the Oto-Zan sanukitoid magma (Fig. 8). Therefore, source heterogeneity beneath Shodo-Shima Island in terms of Sr–Nd–Pb isotopic composition, is suggested to be responsible for the observed isotopic spatial variations.

There is additional evidence suggesting that the HMA magma source beneath Shodo-Shima Island is heterogeneous. It is well established that olivine in the upper mantle possesses rather constant NiO contents of 0·35–0·5 wt %, whereas its Mg-number can be variable (Fig. 4; Sato, 1977; Takahashi, 1990). Some olivines that crystallized from primitive HMAs in the Setouchi volcanic belt, including those on Shodo-Shima Island, have Mg-number and NiO compositions consistent with a mantle signature (Tatsumi & Ishizaka, 1981, 1982*a*, 1982*b*; Tatsumi *et al.*, 2003). Olivine phenocrysts embedded in the Oto-Zan HMA (OTO-1) are characterized by significantly higher NiO contents, up to 0·6 wt % at Mg-number of ~90 (Fig. 4), suggesting the presence of unusually nickeliferous olivine in its source.

The depleted chemical signature, in terms of high Ni contents in olivine, for the Oto-Zan HMA source is reinforced by the composition of spinel inclusions in the olivine. Two types of HMAs are recognized in the Setouchi volcanic belt (Tatsumi, 1982): one with a crystallization sequence of olivine → orthopyroxene (opx-HMA) and the other with olivine → clinopyroxene (cpx-HMA). The results of high-pressure melting experiments (Tatsumi, 1981, 1982) indicate that harzburgitic and lherzolitic peridotites are the melting residues for opx- and cpx-HMA magmas, respectively, leading Tatsumi (1982) to the conclusion that the opx-HMA magmas are produced either by higher degrees of partial melting or from a relatively depleted mantle peridotite source compared with the cpx-HMA magmas. This is consistent with the difference observed in the spinel compositions, with higher Cr/(Cr + Al) for the opx-HMA magmas (Fig. 5a). Although the Oto-Zan HMA is classified, in terms of its phenocryst assemblage and crystallization sequence, as a cpx-HMA, its spinel inclusions have compositions identical to those in opx-HMAs (Fig. 5a and f).

Magmatic differentiation

Fractional crystallization and assimilation

Continuous sampling and analysis of the Oto-Zan lava flow clearly document a variation in mineralogical and chemical compositions within the single lava flow as a function of height from the base (Figs 3 and 9). It may thus be suggested that magmas having different chemistry and mineralogy have contributed to the lava formation.

Andesites forming the lower part of the lava flow are more depleted in Si, Na, K, Rb and Zr, and more enriched in Fe, Mg, Ca and Ni than those from the upper part (Fig. 9). This, together with constant Nd–Pb isotopic compositions throughout the lava flow (Fig. 10) would suggest the derivation of more felsic magmas through fractional crystallization of a hydrous HMA magma such as OTO-1, which occurs at the base of the lava flow. Grove *et al.* (2003) determined the phase relations of an HMA from the Mt Shasta region over a range of pressure and temperature conditions under H_2O-saturated conditions and demonstrated the liquid line of descent through fractional crystallization of such a hydrous HMA magma (Fig. 7a). Their results may be applicable for examining possible magmatic differentiation paths for the Oto-Zan HMA magma. The reasons for

Table 9: Sr–Nd–Pb isotopic compositions

Sample:	OTO-1	OTO-3	OTO-4	OTO-5	OTO-7	OTO-9	SD-303
Height (m):	0	3·0	6·0	12·0	19·0	29·0	80·0
$^{87}Sr/^{86}Sr$	0·705607 ± 11	0·705665 ± 06	0·705680 ± 06	0·705674 ± 07	0·705877 ± 08	0·705579 ± 06	0·705894 ± 11
$(^{87}Sr/^{86}Sr)_t$*	0·70548	0·70553	0·70555	0·70554	0·70573	0·70543	0·70575
$^{143}Nd/^{144}Nd$	0·512590 ± 08	0·512585 ± 12	0·512581 ± 08	0·512561 ± 12	0·512580 ± 10	0·512601 ± 10	0·512587 ± 14
$^{208}Pb/^{204}Pb$	38·645 ± 3	38·648 ± 3	38·651 ± 4	38·650 ± 3	38·625 ± 3	38·611 ± 3	38·626 ± 3
$^{207}Pb/^{204}Pb$	15·607 ± 1	15·608 ± 1	15·609 ± 1	15·608 ± 1	15·601 ± 1	15·599 ± 1	15·601 ± 1
$^{206}Pb/^{204}Pb$	18·385 ± 1	18·387 ± 1	18·386 ± 1	18·386 ± 1	18·380 ± 1	18·374 ± 1	18·385 ± 1

*Corrected to 13 Ma.

believing so are twofold. First, the experimental starting composition was similar to the Oto-Zan HMA composition. Second, the original H_2O content of the Setouchi HMAs (~7 wt %) would cause H_2O-oversaturation in a shallow crustal magma reservoir, which is the condition reproduced by the Grove *et al.* (2003) experiments. A marked increase in FeO*/MgO with increasing SiO_2 content in the differentiated melt was observed in their crystallization experiments (Fig. 7a), which is a trend quite different from that of the Oto-Zan magma differentiation.

In order to further examine the crystallization differentiation process, a simple mass-balance calculation was made assuming an initial composition equal to the HMA OTO-1 and a final composition equal to one of the most differentiated samples within the lava flow (OTO-9). The results indicate that fractionation of plagioclase and magnetite is needed to produce the differentiated magma from the parental HMA (Table 11). However, neither plagioclase nor magnetite is present as a phenocryst phase in the Oto-Zan samples. Petrographic evidence also does not support this simple process. The presence of both normally zoned and reversely zoned pyroxene phenocrysts in a single sample, especially in differentiated rocks, indicates an open-system differentiation process such as mixing of two compositionally different magmas. It may thus be concluded that a fractional crystallization process was not responsible for differentiation of the Oto-Zan magma.

Simultaneous assimilation of crustal materials and fractional crystallization (e.g. DePaolo, 1981; Hildreth & Moorbath, 1988; Dias & Leterrier, 1994) is another possibility for producing differentiated magmas from an HMA magma in the Oto-Zan lava flow, because plagioclase and quartz, which are major constituent minerals in basement granitic rocks, occur ubiquitously, although not voluminously, as xenocrysts in the lava flow (Table 2). A simple mass-balance calculation based on compositions of Oto-Zan lava samples, phenocryst phases and a granite from Shodo-Shima Island (Tatsumi *et al.*, 2002) yields results consistent with assimilation coupled with fractional crystallization (Table 11). However, the isotopic compositions of the Oto-Zan samples and the basement rocks, especially for Pb, do not support this (Fig. 8); a contaminant having a much higher $^{207}Pb/^{204}Pb$ and $^{208}Pb/^{204}Pb$ composition than the Shodo-Shima basement rocks is required for the assimilation process, and there is no evidence for such materials.

Magma mixing

Many calc-alkalic andesites are characterized by the following petrographic and chemical signatures: (1) the presence of reversely zoned pyroxene phenocrysts with rounded cores mantled by rims with higher Mg-number; (2) the presence of plagioclase phenocrysts with a wide range of compositions and with a dusty zone containing fine melt inclusions; (3) the presence of disequilibrium mineral assemblages such as Mg-rich olivine and quartz; (4) linear chemical trends typically demonstrated for MgO and FeO against SiO_2. These observations led several authors (e.g. Eichelberger, 1975; Sakuyama, 1979, 1981; Cribb & Barton, 1997; Hunter, 1998; Rorolo & Castorina, 1998; Feeley *et al.*, 2002; Tatsumi *et al.*, 2002) to the conclusion that mixing of mafic and felsic magmas plays a significant role in the production of calc-alkalic andesite magmas. Orthopyroxene-bearing andesites from the Oto-Zan lava flow, i.e. samples from 19 m above the flow base, contain ortho- and clinopyroxenes that exhibit both normal and reverse zoning (Fig. 6, Tables 5 and 6). Furthermore, the differentiation trends observed for this lava flow are generally linear (Fig. 13). It may thus be suggested that mixing of compositionally different magmas may have played a role in the evolution of the Oto-Zan magma.

A possible, and the most plausible, candidate for the mafic end-member magma would be the HMA OTO-1 sample that forms the basal part of the lava flow. Rhyolites do exist on Shodo-Shima Island and could represent a possible felsic end-member. The compositions of such

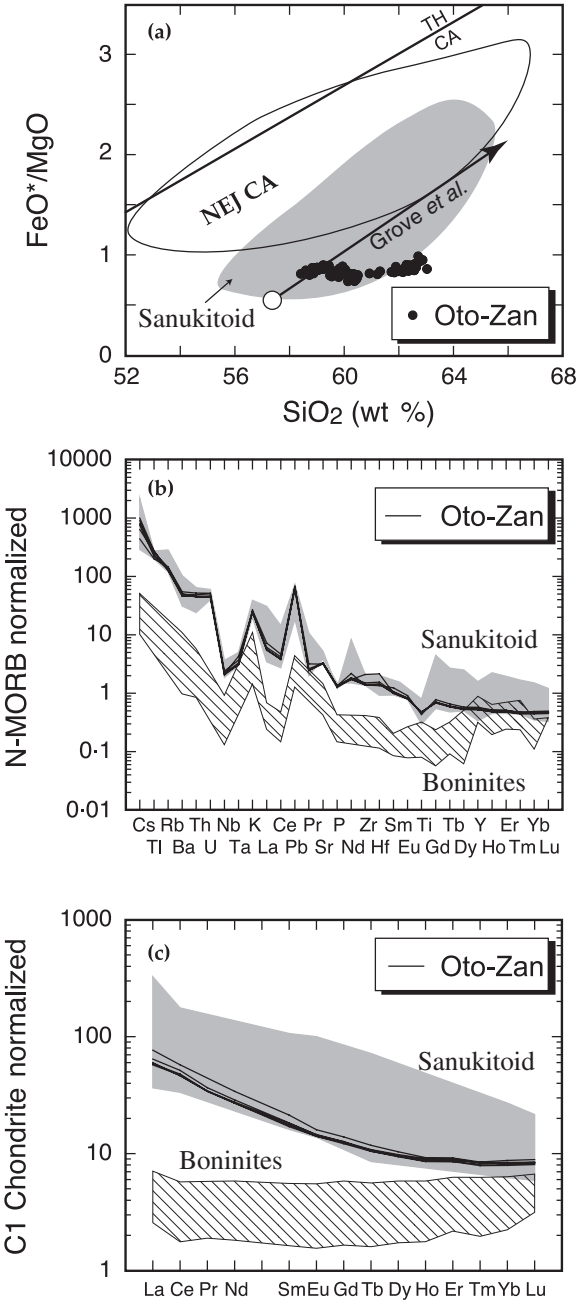

Fig. 7. Geochemical characteristics of sanukitoids from the Oto-Zan lava flow and other regions of the Setouchi volcanic belt (Shimoda *et al.*, 1998; Tatsumi & Ishizaka, 1982*a*, 1982*b*; Tatsumi *et al.*, 2003), boninites (Pearce *et al.*, 1992; Taylor *et al.*, 1994) and Quaternary calc-alkalic volcanic rocks from the NE Japan arc (NEJ CA; Tatsumi & Kogiso, 2003). The liquid line of descent obtained for an HMA from the Shasta region, California (Grove *et al.*, 2003) is shown in (a). Sanukitoids comprising the Oto-Zan lava flow show an extreme calc-alkalic trend and have trace element characteristics identical to those from other regions of the Setouchi volcanic belt and are distinct from boninites. TH, tholeiitic series; CA, calc-alkalic series (Miyashiro, 1974). Normalization values from Sun & McDonough (1989). (a) FeO*/MgO vs wt% SiO_2; (b) N-MORB normalized incompatible element patterns; (c) chondrite-normalized REE patterns. Normalization values from Sun & McDonough (1989).

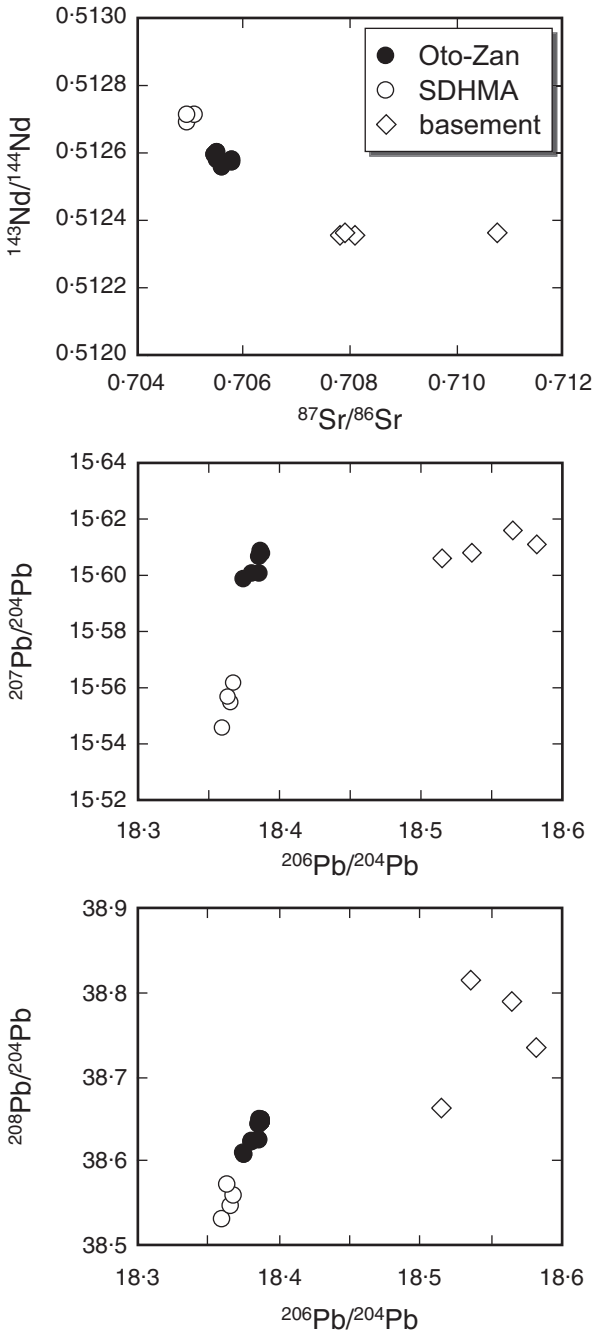

Fig. 8. Sr–Nd–Pb isotopic compositions of the Oto-Zan lava flow, HMAs (SDHMA; Shimoda *et al.*, 1998), and basement rocks (Tatsumi *et al.*, 2002) from Shodo-Shima Island. The isotopic compositions of the Oto-Zan sanukitoids differ from those of the Shodo-Shima HMAs and cannot be explained by crustal contamination of those HMA magmas, suggesting the distribution of highly heterogeneous magma sources beneath Shodo-Shima Island.

rhyolites are shown in Fig. 13, together with those of the Oto-Zan lava flow. Linear chemical trends observed for Oto-Zan sanukitoids, such as those for SiO_2 vs MgO, FeO and Th, can be reasonably explained by the

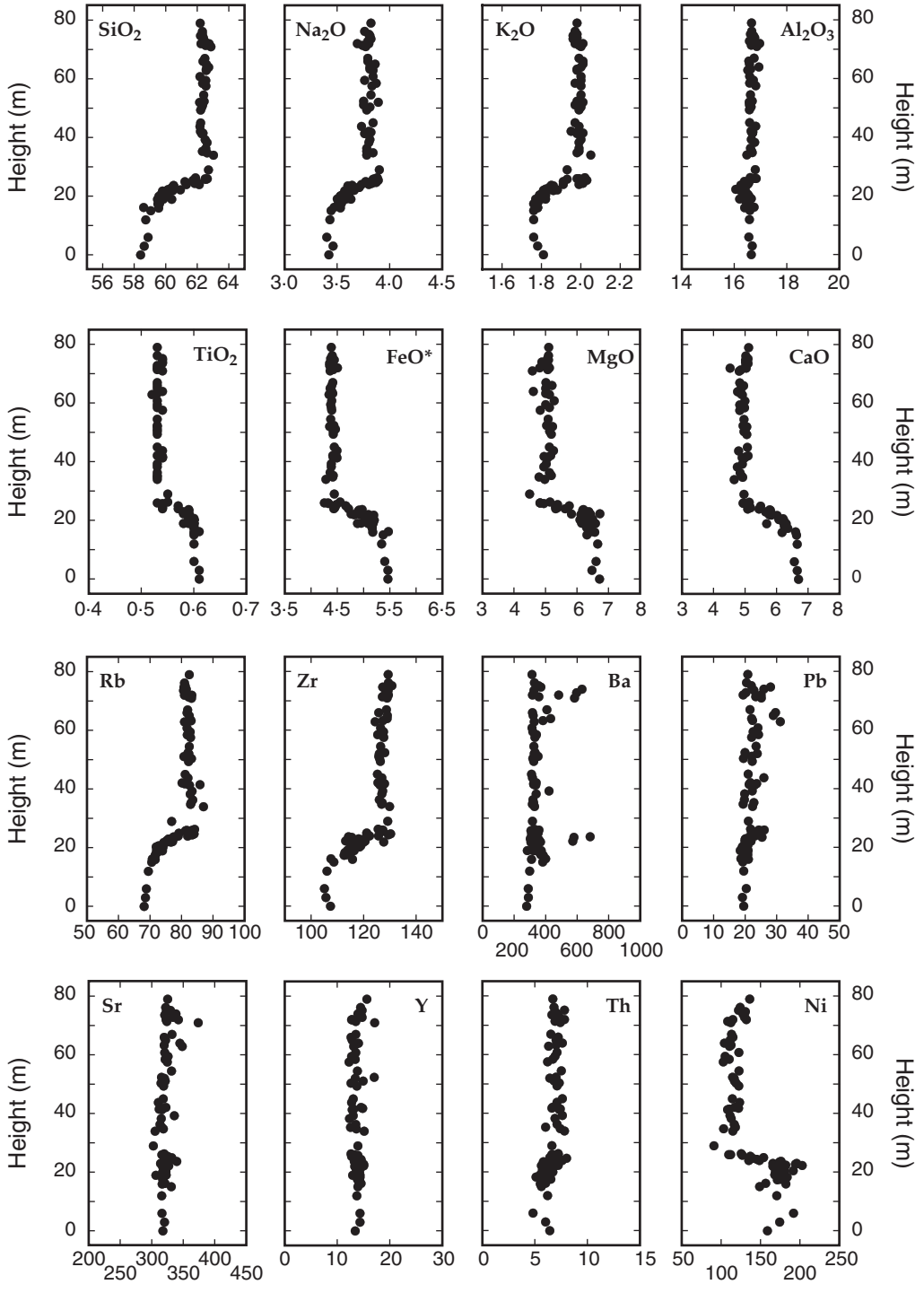

Fig. 9. Variations in element concentrations in the Oto-Zan lava flow as a function of height from the base. Concentrations of most elements change with increasing height synchronously with the changes in modal minerology (cf. Fig. 2), although the abundance of some elements such as Ba, Pb, Sr, Y and Th remains constant throughout the lava flow.

contribution of a Shodo-Shima rhyolite magma as the felsic end-member in a magma mixing process. However, chemical trends for other elements do not support this (Fig. 13).

Alternatively, the relatively constant Sr–Nd–Pb isotopic compositions throughout the lava flow would be consistent with derivation of the felsic end-member magma from the parental Oto-Zan HMA magma,

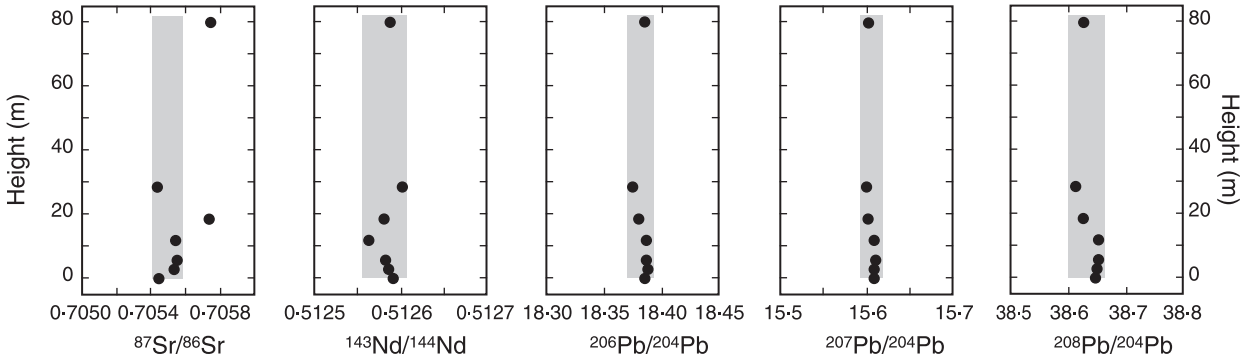

Fig. 10. Variations in Sr–Nd–Pb isotopic ratios in the Oto-Zan lava flow as a function of height from the base. Although some 'spikes' are documented, these isotopic ratios are broadly constant throughout the lava flow (shaded), suggesting a rather closed-system differentiation from a common parental magma for the Oto-Zan sanukitoid samples.

which can be referred as to 'internal mixing' or 'back mixing'. Formation processes of such a differentiated felsic magma are hereafter discussed based on the present experimental results.

Although the compositional trends of melts produced at high temperatures, especially those for TiO_2 and Al_2O_3, are governed by the amount of H_2O in the system, the composition of melts produced at lower temperature (~1000°C) are broadly similar (Fig. 12 and Table 10). This may be attributed to H_2O-saturation in such small-volume, low-temperature, rhyolitic melts, even with different H_2O contents in the overall system, because 4–7 wt % H_2O in a rhyolitic melt (0·7, 1·5 and 2·1 wt % H_2O in the system with 90, 60 and 50% solids and 10, 40 and 50% melt, respectively) may be close to or above the solubility limit of H_2O (Burnham & Nekcasil, 1986; Moore *et al.*, 1998; Yamashita, 1999). It thus seems reasonable to assume a melt with a composition that plots on an extended portion of the liquid line of descent as a possible felsic melt derived from the Oto-Zan HMA magma (Fig. 12). If we accept this as the end-member felsic magma, then the differentiation trends of the Oto-Zan andesites, including the unusually linear trend for MgO and the decrease in TiO_2 with increasing SiO_2, can be successfully explained by mixing of the basal HMA magma with this felsic magma (Fig. 12). However, the behaviour of alkali elements, especially K_2O, is less clear; a felsic magma with a lower concentration of K_2O is required for the end-member component.

One explanation for the discrepancy in K_2O would be the presence of K-bearing minerals as a crystallizing phase. This is likely, because the experimental results suggest that biotite, in addition to amphibole, appears as a subsolidus phase for the HMA composition (Fig. 11 and Table 10).

Plagioclase and Fe–Ti oxides are solid phases well above the solidus of the HMA (Fig. 11), resulting in the production of felsic magmas with characteristic depletions in Ti and Sr, as these partition into Fe–Ti oxide and plagioclase, respectively. The behaviour of Ti and Sr as compatible elements rather than incompatible elements in the Oto-Zan lava flow (Fig. 13) can thus be readily modelled by the involvement of a Ti–Sr-depleted magma as the felsic end-member component during magma mixing.

The mineral assemblage in the solid residue that coexists with rhyolitic melts can also be constrained using the geochemical characteristics of the Oto-Zan lava samples. If we accept the Oto-Zan differentiation trend as a mixing trend, then the composition of the two end-member components should lie on extensions of the linear mixing trends. Assuming that the HMA and felsic components possess SiO_2 contents of 58 and 73 wt %, respectively, other element concentrations can be obtained using the mixing lines (Fig. 10 and Table 12). The rhyolite magma thus calculated exhibits the following chemical characteristics relative to the HMA magma (Fig. 14): (1) for univalent cations, both K and Na are more depleted than Rb; (2) for divalent cations, both Sr and Ba are strongly depleted relative to Pb; and (3) for trivalent cations, Ti is depleted. Based on the crystal structure control in trace element partitioning between solid and melt (Matsui *et al.*, 1977), it may be reasonable to accept that the ionic radii of the elements with significant relative depletions could fit with the sizes of cation sites of plagioclase, amphibole, biotite and magnetite (Fig. 14), suggesting the presence of these phases in the residual solid that coexisted with the rhyolitic melt. This is in harmony with the phases observed in the experimental results.

Formation process of Oto-Zan composite lava

The experimental results, together with the geochemical characteristics of the Oto-Zan lava flow, suggest the involvement of two magmas, one HMA and the other rhyolitic, as end-member components for magma mixing.

Table 10: Results of experiments for Oto-Zan HMA

Run no.	Temp. (°C)	Duration (h)	H_2O (wt %)	Phases identified	Chemical composition										
					Phases	SiO_2	TiO_2	Al_2O_3	FeO*	MnO	MgO	CaO	Na_2O	K_2O	Cr_2O_3	Total
HG266W1	900	75	0·7	gl, pl, bt, amph, mt, il											
HG267W1	950	75	0·7	gl, pl, opx, cpx, mt, il	opx	52·67	0·51	2·73	14·15	0·34	26·34	1·72	0·05	0·05	0·1	98·67
					STD[1]	0·30	0·07	0·14	0·44	0·02	0·53	0·17	0·03	0·02	0·02	
HG240W1	1000	50	0·7	gl, pl, opx, cpx, mt, il	gl	66·24	0·58	14·10	2·38	0·01	1·53	2·31	2·41	5·31	0·03	94·90
					STD[1]	–	–	–	–	–	–	–	–	–	–	
					Corrected[2]	70·22	0·61	14·95	2·52	0·01	1·62	2·45	2·86	4·75		100·00
					mt	0·53	4·48	3·70	75·45	0·31	4·97	0·24	0·01	0·08	0·22	89·99
					STD[1]	0·13	0·10	0·03	0·23	0·02	0·21	0·04	0·01	0·01	0·03	
					il	1·39	21·00	1·52	63·48	0·11	2·90	0·62	0·09	0·11	0·23	91·45
					STD[1]	0·67	0·71	0·39	0·84	0·04	0·40	0·60	0·06	0·03	0·10	
HG255W1	1000	75	0·7	gl, pl, opx, cpx, mt, il	gl	66·42	0·87	14·42	2·39	0·04	0·98	2·39	2·62	5·37	0·02	95·52
					STD[1]	0·26	0·06	0·36	0·18	0·02	0·25	0·25	0·14	0·17	0·01	
					Corrected[2]	69·93	0·92	15·18	2·52	0·04	1·03	2·52	3·09	4·77		100·00
					pl	56·14	0·09	26·19	0·94	0·02	0·29	10·32	4·36	1·10	0·00	99·45
					STD[1]	0·65	0·04	0·50	0·14	0·01	0·24	0·42	0·18	0·17	0·00	
					opx	53·73	0·50	3·24	13·42	0·38	25·51	2·35	0·20	0·09	0·10	99·52
					STD[1]	0·88	0·20	1·40	1·01	0·03	1·22	0·54	0·19	0·06	0·07	
HG254W1	1050	51	0·7	gl, pl, opx, cpx, mt, il	gl	63·91	1·09	14·96	3·49	0·07	1·72	3·57	3·14	4·53	0·01	96·49
					STD[1]	0·28	0·04	0·26	0·09	0·02	0·21	0·10	0·07	0·07	0·02	
					Corrected[2]	66·47	1·13	15·56	3·63	0·07	1·79	3·71	3·66	3·98		100·00
					pl	55·41	0·11	26·78	0·97	0·01	0·28	10·93	4·27	0·88	0·01	99·65
					STD[1]	0·48	0·10	1·06	0·24	0·01	0·13	0·52	0·23	0·32	0·01	
					opx	54·43	0·33	3·53	10·81	0·32	27·68	2·04	0·11	0·09	0·40	99·74
					STD[1]	1·12	0·13	0·84	2·92	0·09	2·49	0·41	0·08	0·06	0·41	
					cpx	52·15	0·73	3·67	7·84	0·28	16·38	18·30	0·44	0·14	0·14	100·07
					STD[1]	0·28	0·14	0·52	0·27	0·03	0·76	0·61	0·04	0·03	0·00	
HG250W1	1100	25	0·7	gl, pl, opx, cpx	gl	60·38	0·94	15·86	4·55	0·08	2·83	5·16	3·20	3·46	0·02	96·48
					STD[1]	0·28	0·04	0·13	0·09	0·02	0·07	0·06	0·11	0·05	0·02	
					Corrected[2]	62·70	0·98	16·47	4·72	0·08	2·94	5·36	3·72	3·03		100·00
					pl	53·42	0·07	27·88	0·72	0·02	0·29	12·20	3·81	0·58	0·01	99·00
					STD[1]	0·26	0·03	0·47	0·13	0·02	0·29	0·36	0·13	0·08	0·02	
					opx	54·31	0·27	2·61	10·00	0·27	28·87	2·27	0·05	0·04	0·28	98·97
					STD[1]	0·56	0·05	0·67	0·21	0·03	0·50	0·40	0·03	0·01	0·08	
					cpx	52·91	0·51	4·13	6·89	0·26	17·88	16·37	0·39	0·27	0·44	100·05
					STD[1]	0·06	0·04	0·06	0·00	0·02	0·25	0·02	0·01	0·10	0·06	
HG261W1	1100	25	0·7	gl, pl, opx, cpx	gl	61·17	0·96	15·45	4·88	0·09	2·49	4·90	3·03	3·90	0·01	96·88
					STD[1]	0·51	0·03	0·09	0·16	0·02	0·05	0·08	0·08	0·06	0·01	
					Corrected[2]	63·31	0·99	15·99	5·05	0·09	2·58	5·07	3·51	3·41		100·00
					pl	54·45	0·04	27·41	0·84	0·01	0·16	11·22	4·07	0·65	0·01	98·86
					STD[1]	0·78	0·02	0·42	0·06	0·01	0·02	0·44	0·21	0·05	0·02	
					opx	54·00	0·26	3·93	10·50	0·26	28·03	2·31	0·07	0·07	0·19	99·62
					STD[1]	1·04	0·04	1·56	0·57	0·04	0·85	0·21	0·03	0·07	0·05	
					cpx	51·10	0·58	4·28	7·98	0·22	17·13	17·42	0·34	0·06	0·24	99·35
					STD[1]	0·57	0·06	0·90	0·45	0·03	0·76	0·90	0·02	0·01	0·06	
HG246W1	1150	6	0·7	gl, pl, opx	gl	57·92	0·68	16·56	4·45	0·11	4·69	6·91	3·16	2·42	0·01	96·91
					STD[1]	0·33	0·03	0·28	0·16	0·03	0·11	0·07	0·05	0·05	0·01	

Table 10: continued

Run no.	Temp. (°C)	Duration (h)	H_2O (wt %)	Phases identified	Chemical composition										
					Phases	SiO_2	TiO_2	Al_2O_3	FeO*	MnO	MgO	CaO	Na_2O	K_2O	Cr_2O_3	Total
					Corrected[2]	59·77	0·70	17·09	4·59	0·11	4·84	7·13	3·65	2·11		100·00
					pl	52·75	0·04	28·61	0·60	0·02	0·48	12·65	3·53	0·43	0·01	99·12
					STD[1]	0·18	0·03	0·46	0·08	0·01	0·34	0·08	0·07	0·04	0·01	
					opx	55·14	0·18	3·39	7·24	0·22	30·76	2·02	0·07	0·06	0·64	99·72
					STD[1]	0·63	0·04	0·85	0·27	0·02	0·72	0·20	0·07	0·05	0·16	
HG236W1	1200	8	0·7	gl, opx	gl	57·44	0·60	16·40	4·20	0·11	6·31	6·98	2·92	2·13	0·03	97·12
					STD[1]	0·23	0·02	0·08	0·08	0·02	0·07	0·08	0·04	0·03	0·02	
					Corrected[2]	59·15	0·62	16·89	4·33	0·11	6·50	7·19	3·37	1·85		100·00
					opx	54·81	0·14	3·05	5·77	0·17	33·03	1·58	0·04	0·04	0·95	99·58
					STD[1]	0·50	0·02	0·53	0·16	0·03	0·32	0·14	0·01	0·01	0·14	
HG267W2	950	75	1·5	gl, pl, opx, cpx, mt, il	gl	63·94	0·41	14·42	1·74	0·03	0·98	2·27	2·92	4·83	0·01	91·55
					STD[1]	0·33	0·02	0·06	0·03	0·01	0·04	0·06	0·02	0·05	0·01	
					Corrected[2]	70·16	0·45	15·82	1·91	0·03	1·08	2·49	3·59	4·47		100·00
					pl	54·11	0·11	25·82	0·86	0·03	0·94	10·89	4·30	0·63	0·01	97·70
					STD[1]	0·23	0·00	0·20	0·07	0·01	0·05	0·04	0·13	0·04	0·01	
					opx	53·45	0·31	3·27	11·55	0·39	28·29	1·61	0·05	0·06	0·09	99·06
					STD[1]	0·61	0·06	0·58	0·78	0·03	0·59	0·19	0·01	0·01	0·02	
HG260W2	980	75	1·5	gl, pl, opx, cpx, mt, il	gl	63·89	0·75	14·79	2·37	0·06	1·19	2·85	2·91	4·66	0·01	93·48
					STD[1]	0·31	0·03	0·19	0·08	0·02	0·24	0·13	0·07	0·14	0·02	
					Corrected[2]	68·63	0·81	15·89	2·55	0·06	1·28	3·06	3·50	4·22		100·00
					pl	54·56	0·11	26·55	0·98	0·01	0·18	10·85	4·21	0·78	0·01	98·24
					STD[1]	1·10	0·05	1·11	0·10	0·01	0·13	0·83	0·29	0·21	0·01	
					opx	54·79	0·14	2·96	6·47	0·19	31·45	1·82	0·03	0·06	0·64	98·55
					STD[1]	0·16	0·02	0·07	0·46	0·02	0·20	0·07	0·01	0·02	0·20	
					cpx	49·29	0·94	4·75	7·13	0·25	14·96	20·77	0·43	0·09	0·04	98·65
					STD[1]	0·41	0·08	0·44	0·33	0·03	0·17	0·34	0·03	0·01	0·03	
					mt	0·34	4·62	4·06	74·34	0·38	4·92	0·19	0·03	0·08	0·46	89·42
					STD[1]	0·08	0·11	0·07	0·42	0·04	0·10	0·04	0·02	0·02	0·30	
					Il	0·27	22·30	1·09	62·48	0·14	2·87	0·23	0·02	0·06	0·06	89·52
					STD[1]	0·11	0·18	0·03	0·32	0·02	0·04	0·07	0·02	0·01	0·03	
HG240W2	1000	50	1·5	gl, pl, opx, cpx, mt, il	gl	64·10	0·55	15·67	2·50	0·05	1·60	3·27	2·98	4·18	0·00	94·90
					STD[1]	0·39	0·05	0·31	0·17	0·03	0·19	0·21	0·04	0·11	0·00	
					Corrected[2]	67·76	0·58	16·56	2·64	0·05	1·69	3·46	3·53	3·73		100·00
					mt	0·51	2·24	4·77	73·83	0·41	7·15	0·18	0·03	0·08	0·68	89·88
					STD[1]	0·11	0·09	0·07	0·54	0·03	0·16	0·04	0·01	0·01	0·14	
					Il	0·45	16·57	1·46	67·45	0·12	3·03	0·22	0·02	0·08	0·27	89·67
					STD[1]	0·149	0·323	0·091	0·716	0·015	0·132	0·028	0·017	0·011	0·156	
HG249W2	1000	50	1·5	gl, pl, opx, cpx, mt, il	gl	62·78	0·88	15·49	2·87	0·06	1·54	3·44	3·20	4·10	0·01	94·37
					STD[1]	0·26	0·04	0·11	0·08	0·02	0·18	0·05	0·06	0·06	0·01	
					Corrected[2]	66·71	0·94	16·46	3·05	0·06	1·64	3·66	3·81	3·68		100·00
					pl	54·91	0·09	26·98	0·96	0·01	0·17	10·57	4·44	0·70	0·01	98·84
					STD[1]	1·00	0·08	0·83	0·20	0·01	0·10	0·68	0·44	0·22	0·02	
					opx	54·03	0·33	2·49	11·47	0·33	28·27	1·68	0·03	0·06	0·09	98·78
					STD[1]	0·95	0·02	0·40	1·04	0·02	1·35	0·28	0·00	0·01	0·02	
					cpx	49·77	0·90	4·63	7·67	0·23	15·09	19·37	0·41	0·08	0·14	98·29
					STD[1]	0·29	0·03	0·31	0·02	0·02	0·16	0·37	0·02	0·01	0·03	

Run no.	Temp. (°C)	Duration (h)	H_2O (wt %)	Phases identified	Chemical composition										
					Phases	SiO_2	TiO_2	Al_2O_3	FeO*	MnO	MgO	CaO	Na_2O	K_2O	Cr_2O_3	Total
HG256W2	1000	50	1·5	gl, pl, opx, cpx, mt, il	gl	64·69	0·74	14·87	2·44	0·06	1·52	3·20	2·88	4·28	0·01	94·69
					STD[1]	0·47	0·07	0·26	0·17	0·02	0·32	0·35	0·08	0·11	0·01	
					Corrected[2]	67·10	0·90	16·11	3·11	0·07	1·52	3·56	3·31	4·31		100·00
					pl	55·42	0·08	26·96	0·97	0·01	0·15	10·63	4·42	0·67	0·02	99·33
					STD[1]	0·84	0·03	0·56	0·05	0·01	0·03	0·48	0·21	0·09	0·02	
					opx	54·60	0·21	5·38	7·50	0·20	28·99	1·84	0·17	0·22	0·57	99·68
					STD[1]	0·91	0·07	1·81	1·67	0·06	2·67	0·13	0·17	0·22	0·31	
					cpx	50·13	0·96	5·04	7·69	0·27	15·35	19·67	0·44	0·10	0·10	99·75
					STD[1]	0·75	0·11	0·83	0·51	0·03	0·51	0·35	0·04	0·03	0·03	
					mt	0·36	2·87	4·40	75·38	0·45	6·93	0·17	0·03	0·07	0·17	90·83
					STD[1]	0·03	0·12	0·05	0·34	0·03	0·07	0·04	0·02	0·01	0·05	
					Il	0·28	17·44	1·37	68·12	0·12	3·04	0·19	0·03	0·06	0·04	90·69
					STD[1]	0·03	0·34	0·04	0·19	0·04	0·05	0·03	0·02	0·01	0·03	
HG254W2	1050	51	1·5	gl, pl, opx, cpx, mt	gl	59·31	0·80	16·10	4·13	0·09	2·52	5·04	3·26	3·19	0·01	94·45
					STD[1]	0·56	0·04	0·13	0·09	0·02	0·15	0·09	0·06	0·05	0·01	
					Corrected[2]	62·87	0·85	17·07	4·38	0·10	2·67	5·34	3·87	2·85		100·00
					pl	52·66	0·06	27·76	1·03	0·01	0·24	12·02	3·96	0·48	0·02	98·24
					STD[1]	0·59	0·03	0·37	0·12	0·01	0·05	0·53	0·24	0·05	0·03	
					opx	52·81	0·29	5·75	9·73	0·26	26·79	2·18	0·14	0·14	0·09	98·18
					STD[1]	0·74	0·07	1·13	0·46	0·03	1·66	0·40	0·09	0·10	0·03	
					cpx	49·94	0·65	5·70	7·14	0·20	15·26	19·76	0·40	0·08	0·17	99·30
					STD[1]	0·56	0·09	0·95	0·27	0·03	0·31	0·28	0·03	0·02	0·02	
					mt	0·63	2·98	7·39	66·84	0·25	6·90	0·24	0·01	0·10	5·42	90·76
					STD[1]	0·13	0·04	0·02	0·15	0·00	0·05	0·04	0·01	0·02	0·03	
HG250W2	1100	25	1·5	gl, pl, opx, cpx	gl	57·40	0·69	16·56	4·86	0·10	3·97	6·53	3·19	2·51	0·02	95·83
					STD[1]	0·23	0·04	0·21	0·07	0·03	0·40	0·10	0·05	0·06	0·02	
					Corrected[2]	59·92	0·72	17·29	5·07	0·10	4·14	6·82	3·73	2·21		100·00
					pl	51·64	0·02	29·53	0·84	0·00	0·33	13·23	3·34	0·31	0·00	99·24
					STD[1]	0·21	0·01	0·35	0·06	0·00	0·19	0·18	0·03	0·03	0·01	
					opx	54·55	0·19	3·44	8·32	0·22	30·23	2·30	0·08	0·06	0·37	99·76
					STD[1]	0·11	0·01	0·14	0·10	0·03	0·33	0·14	0·03	0·03	0·05	
					cpx	52·83	0·30	4·11	5·31	0·18	17·23	18·61	0·41	0·13	0·30	99·41
					STD[1]	0·37	0·02	0·02	0·09	0·01	0·19	0·26	0·04	0·04	0·06	
HG261W2	1100	25	1·5	gl, pl, opx, cpx	gl	58·66	0·78	15·82	4·68	0·10	3·22	5·84	3·03	2·91	0·01	95·05
					STD[1]	0·39	0·04	0·17	0·13	0·02	0·08	0·10	0·06	0·06	0·02	
					Corrected[2]	61·78	0·82	16·66	4·93	0·11	3·39	6·15	3·57	2·59		100·00
					pl	52·83	0·05	27·91	1·02	0·01	0·18	12·22	3·68	0·41	0·01	98·32
					STD[1]	0·55	0·02	0·26	0·05	0·02	0·01	0·23	0·11	0·03	0·01	
					opx	53·81	0·18	4·20	8·03	0·21	30·42	1·95	0·05	0·04	0·17	99·06
					STD[1]	0·81	0·03	0·85	0·42	0·03	0·52	0·21	0·02	0·02	0·05	
					cpx	49·93	0·50	5·18	6·56	0·19	16·31	19·06	0·36	0·06	0·24	98·39
					STD[1]	0·72	0·06	0·74	0·28	0·02	0·40	0·56	0·06	0·05	0·10	
HG236W2	1200	8	1·5	gl	gl	56·49	0·61	15·76	4·79	0·10	6·81	6·70	2·82	2·06	0·03	96·17
					STD[1]	0·17	0·03	0·03	0·08	0·02	0·07	0·07	0·07	0·04	0·02	
					Corrected[2]	58·75	0·63	16·39	4·98	0·10	7·08	6·97	3·28	1·81		100·00

Table 10: continued

Run no.	Temp. (°C)	Duration (h)	H_2O (wt %)	Phases identified	Chemical composition										
					Phases	SiO_2	TiO_2	Al_2O_3	FeO*	MnO	MgO	CaO	Na_2O	K_2O	Cr_2O_3	Total
HG266W3	900	75	2·1	gl, pl, amph, mt, il	amph	43·87	1·75	11·12	9·24	0·16	15·91	11·16	1·62	0·86	0·09	95·77
					STD[1]	0·52	0·30	0·52	0·67	0·03	0·49	0·40	0·07	0·19	0·03	
HG267W3	950	75	2·1	gl, pl, opx, amph, mt, il	pl	52·54	0·06	26·49	1·01	0·01	0·66	11·16	3·87	0·58	0·00	96·39
					STD[1]	0·26	0·04	0·39	0·02	0·01	0·10	0·20	0·10	0·12	0·01	0·42
					opx	53·14	0·29	3·69	8·63	0·37	29·92	1·54	0·11	0·11	0·06	97·88
					STD[1]	0·38	0·06	0·40	0·42	0·02	0·66	0·36	0·07	0·06	0·05	0·24
					amph	42·15	2·10	11·76	9·20	0·13	15·90	11·04	1·92	0·90	0·09	95·19
					STD[1]	0·48	0·20	0·48	0·75	0·02	0·19	0·23	0·05	0·04	0·03	0·36
HG260W3	980	75	2·1	gl, pl, opx, cpx, mt, il	gl	61·52	0·74	15·73	2·54	0·05	1·55	3·58	3·09	3·91	0·01	92·72
					STD[1]	0·53	0·03	0·10	0·07	0·02	0·05	0·06	0·08	0·06	0·02	
					Corrected[2]	66·53	0·80	17·01	2·75	0·05	1·68	3·87	3·74	3·57		100·00
					pl	53·94	0·05	27·30	0·88	0·01	0·11	11·24	4·42	0·47	0·01	98·43
					STD[1]	0·85	0·02	0·48	0·06	0·02	0·02	0·61	0·31	0·05	0·02	
					opx	53·61	0·34	3·39	9·40	0·35	29·51	1·80	0·05	0·07	0·08	98·60
					STD[1]	0·81	0·08	0·67	0·69	0·03	0·79	0·52	0·03	0·04	0·03	
					cpx	49·23	0·83	5·49	6·81	0·22	15·20	20·42	0·42	0·08	0·10	98·80
					STD[1]	0·95	0·06	1·23	0·52	0·02	0·50	0·84	0·02	0·03	0·02	
					mt	0·35	3·44	5·09	72·23	0·36	6·16	0·18	0·02	0·08	1·42	89·33
					STD[1]	0·07	0·09	0·06	0·70	0·02	0·07	0·04	0·02	0·01	0·69	
					Il	0·16	21·01	1·24	63·35	0·11	3·21	0·15	0·01	0·05	0·16	89·45
					STD[1]	0·02	0·13	0·01	0·17	0·02	0·05	0·02	0·01	0·01	0·04	
HG240W3	1000	50	2·1	gl, pl, opx, cpx, mt, il	gl	62·08	0·61	16·24	2·68	0·07	2·14	3·88	2·90	3·45	0·01	94·06
					STD[1]	0·38	0·05	0·21	0·09	0·02	0·42	0·10	0·40	0·10	0·01	
					Corrected[2]	66·14	0·65	17·30	2·86	0·07	2·28	4·13	3·46	3·10		100·00
					pl	52·96	0·10	27·73	1·24	0·01	0·97	12·04	3·50	0·53	0·00	99·08
					STD[1]	0·22	0·04	0·44	0·05	0·01	0·57	0·42	0·08	0·05	0·00	
					opx	53·74	0·28	3·83	9·32	0·30	31·27	1·42	0·04	0·05	0·11	100·36
					STD[1]	0·42	0·02	0·33	1·12	0·03	1·20	0·20	0·01	0·01	0·01	
					cpx	49·54	0·88	5·17	6·96	0·21	16·01	20·02	0·43	0·07	0·13	99·42
					STD[1]	0·64	0·14	0·56	0·34	0·04	0·84	0·78	0·06	0·02	0·04	
					mt	0·63	1·74	5·54	72·07	0·42	8·48	0·17	0·02	0·09	1·16	90·32
					STD[1]	0·07	0·14	0·09	0·32	0·02	0·16	0·04	0·02	0·02	0·21	
					Il	0·56	15·04	1·56	68·43	0·12	3·15	0·29	0·02	0·08	0·32	89·57
					STD[1]	0·19	0·50	0·05	0·65	0·02	0·11	0·08	0·02	0·02	0·09	
HG255W3	1000	75	2·1	gl, pl, opx, cpx, mt, il	gl	60·77	0·76	16·14	3·12	0·07	1·87	4·19	3·18	3·42	0·01	93·53
					STD[1]	0·21	0·05	0·11	0·07	0·03	0·07	0·07	0·05	0·05	0·01	
					Corrected[2]	65·09	0·81	17·29	3·34	0·07	2·00	4·49	3·81	3·09		100·00
					pl	53·21	0·05	28·07	0·99	0·01	0·18	12·13	4·04	0·41	0·01	99·10
					STD[1]	0·81	0·03	0·58	0·14	0·01	0·06	0·72	0·34	0·04	0·01	
					opx	52·91	0·26	5·08	9·68	0·30	28·07	1·45	0·07	0·11	0·09	98·02
					STD[1]	1·04	0·07	1·51	0·49	0·02	0·99	0·19	0·04	0·06	0·03	
					cpx	49·43	0·71	5·60	7·06	0·21	14·89	20·42	0·42	0·07	0·08	98·89
					STD[1]	0·86	0·08	1·08	0·49	0·02	0·42	0·72	0·02	0·01	0·05	

Run no.	Temp. (°C)	Duration (h)	H_2O (wt %)	Phases identified	Chemical composition										
					Phases	SiO_2	TiO_2	Al_2O_3	FeO*	MnO	MgO	CaO	Na_2O	K_2O	Cr_2O_3	Total
HG254W3	1050	51	2·1	gl, pl, opx, cpx, mt	gl	58·29	0·73	16·66	4·13	0·09	2·86	5·59	3·22	2·83	0·01	94·41
					STD[1]	0·29	0·04	0·12	0·09	0·02	0·04	0·07	0·06	0·05	0·01	
					Corrected[2]	61·78	0·77	17·66	4·38	0·10	3·03	5·93	3·82	2·53		100·00
					pl	52·24	0·04	28·94	0·89	0·02	0·20	13·09	3·62	0·31	0·01	99·36
					STD[1]	0·55	0·03	0·30	0·08	0·02	0·02	0·40	0·20	0·03	0·01	
					opx	53·19	0·23	5·85	8·81	0·24	28·96	1·68	0·06	0·07	0·13	99·22
					STD[1]	0·81	0·04	1·11	0·38	0·03	0·42	0·20	0·02	0·01	0·07	
					cpx	49·48	0·63	6·56	6·90	0·17	15·07	20·22	0·37	0·08	0·17	99·65
					STD[1]	0·44	0·09	0·51	0·23	0·03	0·40	0·64	0·01	0·02	0·09	
					mt	0·49	2·39	8·95	63·95	0·30	7·60	0·17	0·03	0·10	6·32	90·30
					STD[1]	0·20	0·07	0·24	0·64	0·03	0·47	0·02	0·02	0·01	0·09	
HG261W3	1100	25	2·1	gl, opx, cpx	gl	55·92	0·59	16·55	4·85	0·09	4·24	7·01	2·86	2·36	0·01	94·48
					0·31	0·03	0·12	0·08	0·03	0·06	0·07	0·07	0·03	0·02		
					Corrected[2]	59·21	0·62	17·52	5·14	0·10	4·49	7·42	3·39	2·11		100·00
					opx	53·21	0·19	4·95	7·22	0·20	30·96	1·79	0·04	0·03	0·16	98·75
					STD[1]	0·70	0·05	0·77	0·18	0·02	0·53	0·21	0·02	0·01	0·07	
					cpx	49·54	0·44	5·46	6·38	0·15	15·94	20·15	0·35	0·04	0·46	98·91
HG246W3	1150	6	2·1	gl, opx, ol	STD[1]	0·48	0·04	0·15	0·20	0·02	0·40	0·45	0·02	0·01	0·09	
					gl	56·35	0·58	15·97	5·14	0·10	6·00	6·86	2·86	2·07	0·01	95·94
					STD[1]	0·19	0·04	0·10	0·08	0·03	0·07	0·09	0·05	0·04	0·02	
					Corrected[2]	58·73	0·60	16·64	5·36	0·10	6·25	7·15	3·34	1·82		100·00
					opx	55·99	0·13	2·69	6·17	0·19	32·77	1·39	0·06	0·08	0·67	100·14
					STD[1]	0·32	0·01	0·20	0·26	0·01	0·38	0·11	0·05	0·05	0·16	
					ol	41·07	0·01	0·05	8·24	0·21	50·31	0·18	0·00	0·03	0·03	100·13
					STD[1]	–	–	–	–	–	–	–	–	–	–	
HG236W3	1200	8	2·1	gl	gl	55·58	0·58	15·61	5·18	0·10	6·68	6·58	2·79	2·04	0·03	95·17
					STD[1]	0·22	0·02	0·06	0·08	0·03	0·08	0·07	0·06	0·04	0·02	
					Corrected[2]	58·41	0·61	16·40	5·44	0·11	7·02	6·91	3·28	1·81		100·00

gl, glass; pl, plagioclase; bt, biotite; amph, amphibole; mt, magnetite; il, ilmenite; opx, orthopyroxene; cpx, clinopyroxene; FeO*, total iron as FeO; ol, olivine.
[1]Standard deviation (1σ); [2]'corrected' melt compositions.

Here, we discuss the mechanisms for both production and mixing of these two magmas and propose a possible model for formation of the Oto-Zan composite lava flow (Fig. 15).

Solidification of HMA magma and remelting of HMA pluton

A significant dilemma is the almost anhydrous nature of the Oto-Zan sanukitoids, as the HMA magma produced in the uppermost mantle contains ~7 wt % H_2O. If H_2O was released from the HMA magma by vapor-saturation via magmatic ascent, then HMA sanukitoid may contain a large amount of phenocrysts as observed in boninites. However, Setouchi HMAs are phenocryst-poor.

A potential mechanism to resolve this apparent paradox is remobilization and remelting of an andesitic pluton, as proposed by Sparks and co-workers (Matthews *et al.*, 1999; Murphy *et al.*, 2000; Couch *et al.*, 2001) to account for the characteristic mineral disequilibrium often observed in calc-alkalic andesites. Tamura & Tatsumi (2002) and Tamura *et al.* (2003) suggested that felsic rocks in the Izu–Bonin arc and aphyric andesites from Daisen volcano could be produced by such a process. Production of the Oto-Zan lava flow showing the petrographical and geochemical characteristics described here may be also attributed to the remelting of a solidified HMA magma.

In this scenario, the original Oto-Zan magma, inferred to have been a mantle-derived HMA magma that last

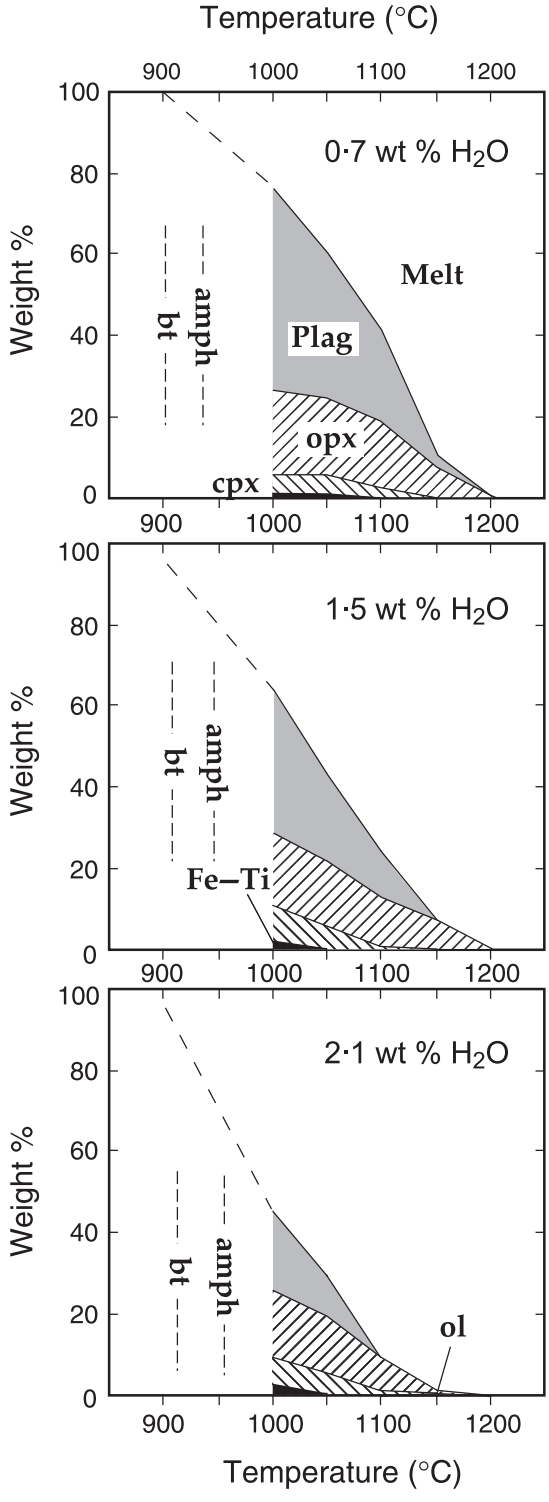

Fig. 11. Modal minerology of experimental run products estimated from mass balance calculations and phase compositions. Although amphibole and biotite are present in the low-T run products, modal proportions could not be estimated because of the absence of phases of analysable size. Plag, plagioclase; opx, orthopyroxene; cpx, clinopyroxene; Fe–Ti, magnetite and/or ilmenite; ol, olivine; amph, amphibole; bt, biotite.

equilibrated with the upper mantle immediately beneath the Moho in the presence of ~7 wt % H_2O, would have undergone extensive crystallization, probably resulting in the formation of an HMA pluton within the crust (Fig. 15a and b). Most of the H_2O originally present in the primary HMA magma should have been extracted from the system through this solidification (Fig. 15b). The present experimental results suggest that the total H_2O content in the solidified HMA pluton would have been significantly smaller than the original magma—probably less than 1 wt %.

Basalt magmas were also produced in the Setouchi volcanic belt. Primitive basalts with compositions that could be in equilibrium with mantle lherzolite phases at uppermost mantle pressures and 1200–1300°C in the presence of <4 wt % H_2O (Tatsumi, 1982) occur on Shodo-Shima Island. It thus seems likely that such a high-temperature basalt magma may have intruded into the base of the postulated HMA pluton, causing remobilization and further melting of the pluton. Such a process was examined, theoretically, by Huppert & Sparks (1988*a*, 1988*b*). We here consider a layer of hot basaltic magma with an initial thickness of D, and a temperature of $T_b(0) = 1300$°C, which is emplaced beneath the HMA pluton with a temperature of $T_p = 900$°C and an interface temperature of T_i (Fig. 16a). The pluton has a solidus temperature (T_m) of 900°C (cf. Fig. 11) and injection of basaltic magma at its base forms a molten layer with a thickness of a (Fig. 16a). Initially, the andesitic magma layer formed at the base of the HMA pluton is stable to convection and transfers heat by conduction. When the Rayleigh number of the melt layer exceeds a critical value of ~2000, convection in the melt layer is then initiated. In the present case, the duration of conductive heat transfer is limited to ~1 day.

The heat flux into the andesitic layer (F_a) has to be equal to the heat flux out of the basaltic layer (F_b):

$$F_a = \rho_a c_a \mathcal{J}_a (T_i - T_a)^{4/3} = F_b = \rho_b c_b \mathcal{J}_b (T_b - T_i)^{4/3} \quad (1)$$

where $\mathcal{J}$ ($\mathcal{J}_a$ and $\mathcal{J}_b$, for andesite and basalt, respectively) is defined by

$$\mathcal{J} = 0.1(\alpha g \kappa^2/\nu)^{1/3} \quad (2)$$

where α is the coefficient of thermal expansion, g the gravitational acceleration, κ the thermal diffusivity and ν the kinematic viscosity.

We then deduce that

$$T_i = (T_b + \gamma T_a)/(1 + \gamma) \quad (3)$$

where

$$\gamma = (\rho_a c_a \mathcal{J}_a / \rho_b c_b \mathcal{J}_b)^{3/4}. \quad (4)$$

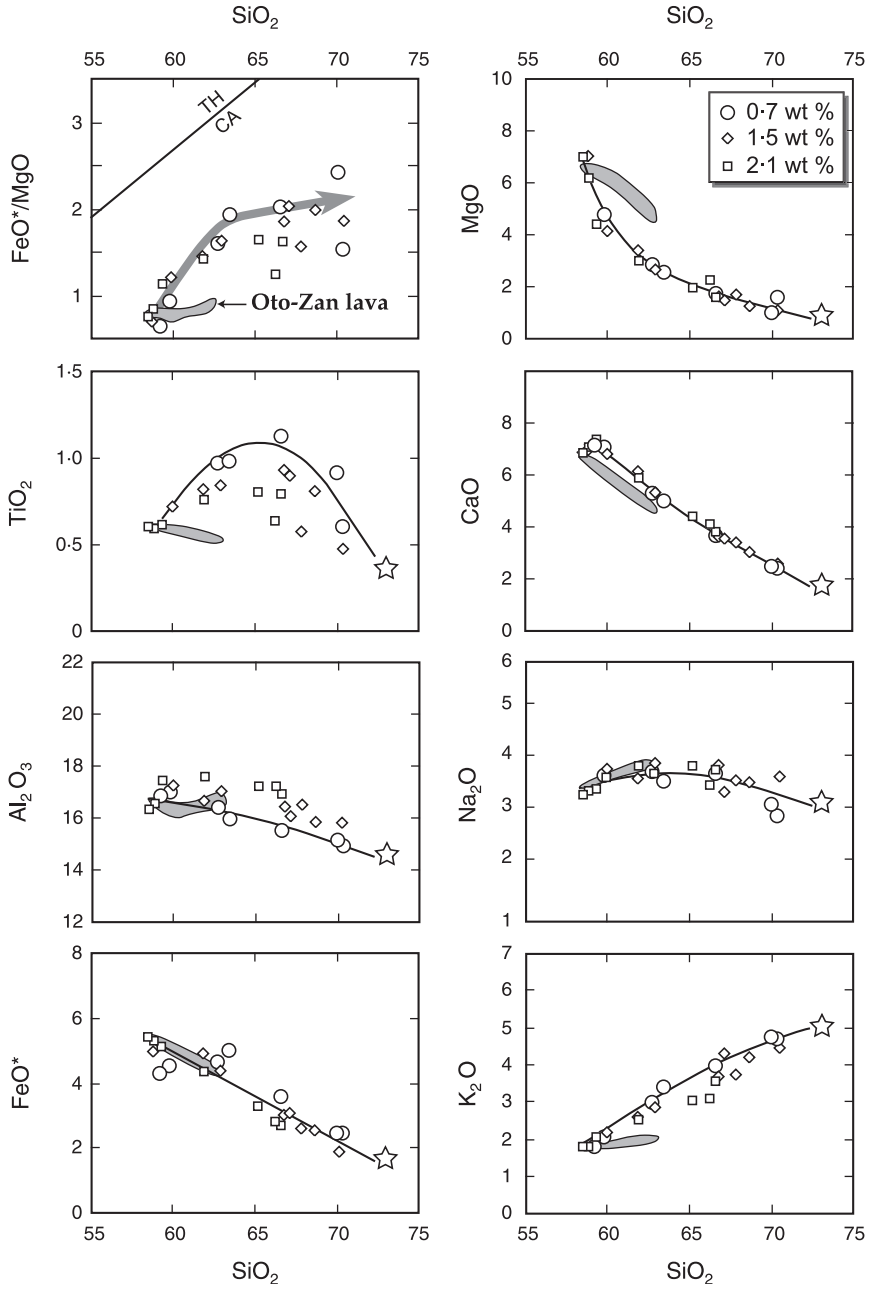

Fig. 12. Comparison of the compositions of the quenched experimental melts and the Oto-Zan lava. The liquid line of descent for the Oto-Zan HMA (continuous lines for 0·7 wt % H_2O experiments), which is similar to that of a Mt Shasta HMA (grey arrow in the FeO*/MgO diagram) from Grove *et al.* (2002), cannot explain the differentiation trend of the Oto-Zan magmas. Instead, mixing between an HMA magma and a highly differentiated rhyolitic magma (star) can reproduce the Oto-Zan trend. However, a felsic magma with a much lower concentration of K_2O, which can be produced in the presence of biotite, is required for the end-member component (see text). TH, tholeiitic series; CA, calc-alkalic series (Miyashiro, 1974); FeO*, total iron as FeO.

Conservation of heat in the basaltic and andesitic melt layers requires that

$$\frac{dT_b}{dt} = -(\mathcal{J}_b/D)(T_b - T_i)^{4/3}/[1 - L_b c_b^{-1}\chi'_b(T_b)] \quad (5)$$

$$\frac{dT_a}{dt} = (\mathcal{J}_a/a)\left\{[(T_i - T_a)^{4/3} - (T_a - T_m)^{4/3}] - \frac{da}{dt}[T_a - T_m - L_a c_a^{-1} - \chi_a(T_a)]\right\}/[1 - L_a c_a^{-1} - \chi'_a(T_a)] \quad (6)$$

Table 11: Results of mass-balance calculation

	SiO_2	TiO_2	Al_2O_3	FeO*	MnO	MgO	CaO	Na_2O	K_2O	P_2O_5	Fraction
Fractional crystallization											
OTO-1	58·4	0·6	16·6	5·4	0·1	6·7	6·7	3·4	1·8	0·2	1
Olivine	40·6	0·0	0·0	9·9	0·0	49·4	0·2	0·0	0·0	0·0	−0·047
Augite	52·5	0·0	5·0	3·0	0·0	15·5	23·0	1·0	0·0	0·0	−0·055
Plagioclase	48·2	0·0	33·2	0·0	0·0	0·0	16·1	2·5	0·0	0·0	−0·098
Magnetite	0·0	14·4	3·3	77·9	0·0	4·4	0·0	0·0	0·0	0·0	−0·018
Result	62·6	0·4	16·7	4·3	0·1	4·4	4·9	4·0	2·3	0·2	0·782
OTO-9	62·7	0·5	16·8	4·4	0·1	4·5	5·0	3·9	1·9	0·2	
Residual	0·2	0·1	0·1	0·1	−0·1	0·1	0·0	−0·1	−0·4	0·0	$R^2 = 0·22$
Assimilation and fractional crystallization											
OTO-1	58·4	0·6	16·6	5·4	0·1	6·7	6·7	3·4	1·8	0·2	1
Olivine	40·6	0·0	0·0	9·9	0·0	49·4	0·2	0·0	0·0	0·0	−0·014
Augite	52·5	0·0	5·0	3·0	0·0	15·5	23·0	1·0	0·0	0·0	−0·046
Granite	75·1	0·1	14·0	1·2	0·0	0·1	1·3	3·9	4·2	0·0	0·272
Result	62·6	0·5	16·7	4·5	0·1	4·4	4·9	3·7	2·4	0·1	1·212
OTO-9	62·7	0·5	16·8	4·4	0·1	4·5	5·0	3·9	1·9	0·2	
Residual	0·1	0·0	0·1	−0·1	0·0	0·1	0·0	0·2	−0·5	0·0	$R^2 = 0·36$

where $\chi_a(T_a)$ is the crystal content of the andesitic magma layer and $\chi_a'(T_a)$ is its derivative with respect to temperature. Conservation of heat at the andesitic pluton–melt interface can be expressed (Huppert, 1986) as

$$\frac{\mathrm{d}a}{\mathrm{d}t} = \frac{c_a \mathcal{J}_a (T_a - T_m)^{4/3}}{c_a (T_m - T_o) + L_a}. \quad (7)$$

Using reasonable values and empirical formulae for the physical parameters (Table 13), the temporal variation of the temperatures of basalt and andesite magma layers for a 500 m thick sill emplaced at the base of the HMA pluton is calculated (Fig. 16b). In this case, totally molten HMA melt is produced at the base of the andesite layer, as the interface temperature (T_i) is higher than the HMA liquidus (1200°C) for the first ~10 years (Fig. 16b). The duration of such total melting depends on the thickness of the basalt layer (Fig. 16c). The thickness of the andesitic, thermal boundary layer increases with time and reaches ~300 m with T_i greater than 1200°C (Fig. 16d). It may, thus, be suggested that the secondary, H_2O-deficient HMA melt can be produced by total melting of the HMA pluton triggered by high-temperature basalt magma injection.

The above consideration based on Huppert & Sparks (1988*a*, 1988*b*) is most applicable when the basalt magma is convecting. Marsh (1989) suggested that convection in basalt magma that intrudes into the crust, and melting of its roof, is only possible under limited conditions such as unusually high temperature for the roof material. In the present model, we assumed that the HMA pluton had an initial temperature of 900°C—much higher than the normal crust temperature (~500°C: Huppert & Sparks, 1988*b*). The present modelling may, thus, provide a reasonable explanation for remelting of the HMA pluton.

Self-mixing in a remolten HMA pluton

Rayleigh–Taylor instability along the thermal boundary layer at the base of the HMA pluton would have caused upwelling of a plume or plumes (Fig. 15c). This HMA plume would have risen into the overlying partially molten HMA pluton, entraining interstitial rhyolitic melts and causing 'self mixing' (Couch *et al.*, 2001) of these magmas to produce a mixed magma (Fig. 15d). Minerals present in the overlying HMA pluton, which may also have been entrained into the rising HMA plume, would have had compositions in disequilibrium with the host mixed melt, which had a higher temperature and more mafic composition than the interstitial rhyolitic melts. It is thus likely that resorption and/or overgrowth of reversely zoned mantles on the entrained minerals would have taken place. No plagioclase phenocrysts are present in the Oto-Zan lava flow, whereas the postulated HMA pluton would have contained plagioclase, suggesting the resorption of plagioclase in the mixed magma. On the other hand, the mixed magma would have been

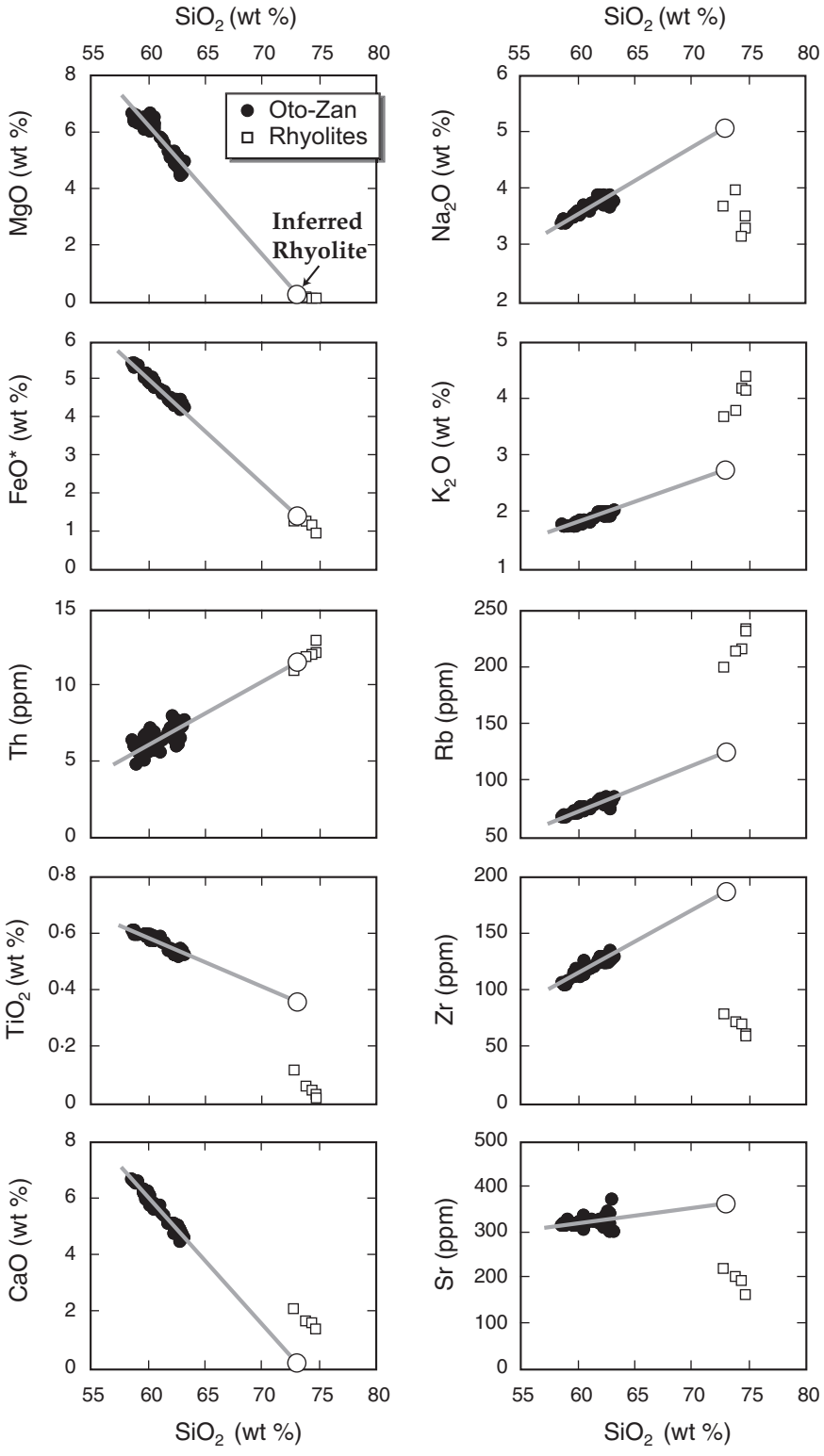

Fig. 13. Chemical differentiation trends for the Oto-Zan sanukitoid samples. The highly linear trends observed can be explained by mixing of two magmas: one having a composition close to the least differentiated Oto-Zan HMA and the other with a rhyolitic composition (open circle). Rhyolites on Shodo-Shima Island, also belonging to the Setouchi volcanic rocks, are not a suitable candidate for the felsic end-member, as the rhyolite compositions do not match those of the inferred rhyolite (see text).

Table 12: Composition of inferred end-member magmas

	HMA	Rhyolite
SiO_2	58·00	73·00
TiO_2	0·63	0·30
Al_2O_3	16·35	17·33
FeO*	5·57	1·58
MnO	0·12	0·00
MgO	7·15	0·02
CaO	6·92	0·15
Na_2O	3·40	4·81
K_2O	1·70	2·68
P_2O_5	0·16	0·14
Ba	336	422
Pb	19	34
Th	5	11
Rb	67	118
Sr	317	341
Zr	106	179

*Total iron as FeO.

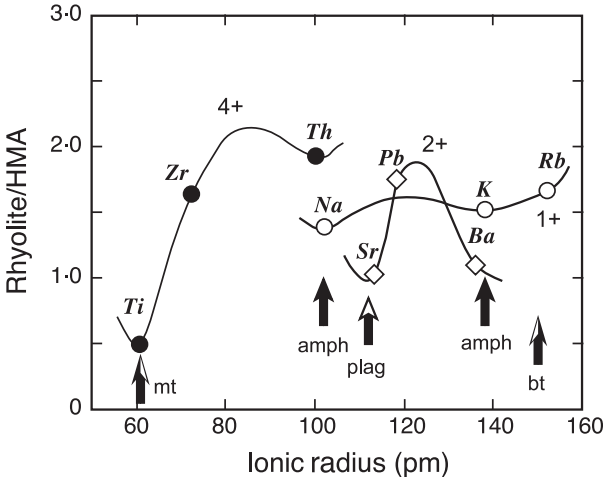

Fig. 14. Incompatible element abundances in the inferred rhyolite end-member relative to those in an HMA as a function of ionic radius and charge. The characteristic element patterns suggest the presence of magnetite (mt), amphibole (amph), biotite (bt) and plagioclase (pl) in the melting residue.

saturated with clino- and orthopyroxene. The experimental results indicate that residual pyroxene in the HMA pluton would have Mg-number lower than the pyroxenes that crystallized from the Oto-Zan HMA and the mixed magmas, suggesting the formation of reversely zoned pyroxene. This is consistent with petrographic observations for the Oto-Zan sanukitoids.

Table 13: Value and formula of physical parameters used in calculations

α	thermal expansion coefficient	5×10^{-5} K^{-1}
g	gravitational acceleration	9·81 m s^{-1}
κ	thermal diffusivity	8×10^{-7} m^2 s^{-1}
ρ_b	density (basalt melt)	$2{\cdot}7 \times 10^3$ kg m^{-3}
ρ_a	density (HMA melt)	$2{\cdot}5 \times 10^3$ kg m^{-3}
C_p	specific heat	$1{\cdot}34 \times 10^3$ J kg^{-1} K^{-1}
L_b	latent heat of crystallization (basalt)	$4{\cdot}2 \times 10^5$ J kg^{-1}
L_a	latent heat of crustallization (HMA)	$2{\cdot}9 \times 10^5$ J kg^{-1}
χ_b	crystal content (basalt)	$6500/T-5$
χ_α	crystal content (HMA)	$-T/300+4$
ν_b	kinematic viscosity (basalt)	$10^{-1} \times (1-1{\cdot}67\chi_b)^{-2{\cdot}5}$ m^2 s^{-1}
ν_a	kinematic viscosity (HMA)	$5 \times 10^{-1} \times (1-1{\cdot}67\chi_a)^{-2{\cdot}5}$ m^2 s^{-1}

The molten plume(s) would have risen to the top of the pluton and formed a zoned magma reservoir in which unmodified HMA magmas and highly mixed, more felsic magmas were situated at the base and top, respectively (Fig. 15d), because of the density difference of these magmas. Once a conduit was established from the top of the zoned magma reservoir, the magmas would have risen via the conduit. During this uprise, the HMA magma, which was originally located at the lowermost part of the reservoir, may have outrun the felsic magma, as it would have had a lower viscosity (Fig. 15e). The emplacement of such HMA magmas followed by more felsic magmas by this mechanism can reasonably explain the petrographical and geochemical characteristics of Oto-Zan composite lava flow (Fig. 15f).

CONCLUSIONS

The Oto-Zan lava flow on Shodo-Shima island in the Setouchi volcanic belt, SW Japan forms a composite lava flow with continuous and systematic changes in both petrographical and geochemical characteristics. The basal part of the lava flow is composed of little differentiated HMA, which grades into more differentiated sanukitoids with increasing height. The more differentiated sanukitoids show petrographic evidence for magma mixing, which is also supported by the liquid lines of descent obtained for the Oto-Zan HMA.

The solidification of a mantle-derived, hydrous HMA magma and remelting of such an HMA pluton through basal heating by a high-T basalt magma played a key role in the formation of the Oto-Zan sanukitoid composite lava flow, including an HMA. Extraction of H_2O in association with pluton solidification may reasonably explain the paradox of sanukitoid and Setouchi HMA

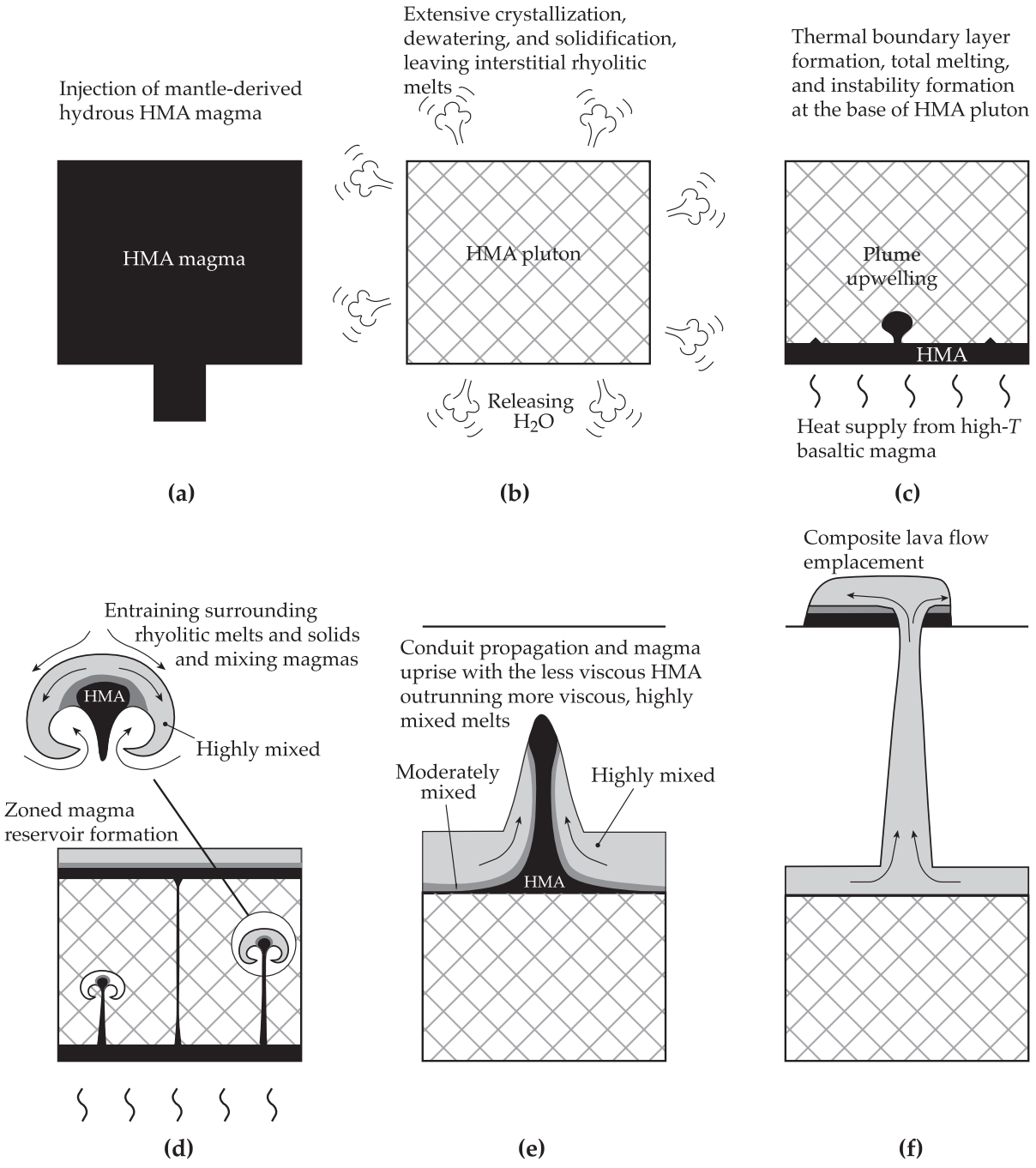

Fig. 15. A possible model for the formation of the Oto-Zan sanukitoids and composite lava flow. A mantle-derived, hydrous HMA magma (a) is likely to crystallize extensively and solidify to release H_2O within the crust (b). Intrusion of a high-*T* basalt magma causes total melting at the base of the HMA pluton to produce a dry HMA magma (c), which rises to entrain interstitial rhyolitic melts remaining in the upper part of the HMA pluton (d). Formation of a zoned magma reservoir (e) and subsequent eruption of that reservoir formed the Oto-Zan composite lava flow (f).

genesis, i.e. although they are originally derived from mantle-derived hydrous HMA magmas, they are rather aphyric and H_2O-poor. Remelting of the HMA pluton resulted in total melting of the basal part of the pluton to produce an H_2O-deficient HMA, which would have risen within the pluton and mixed with interstitial rhyolitic melts, resulting in the formation of a zoned magma reservoir.

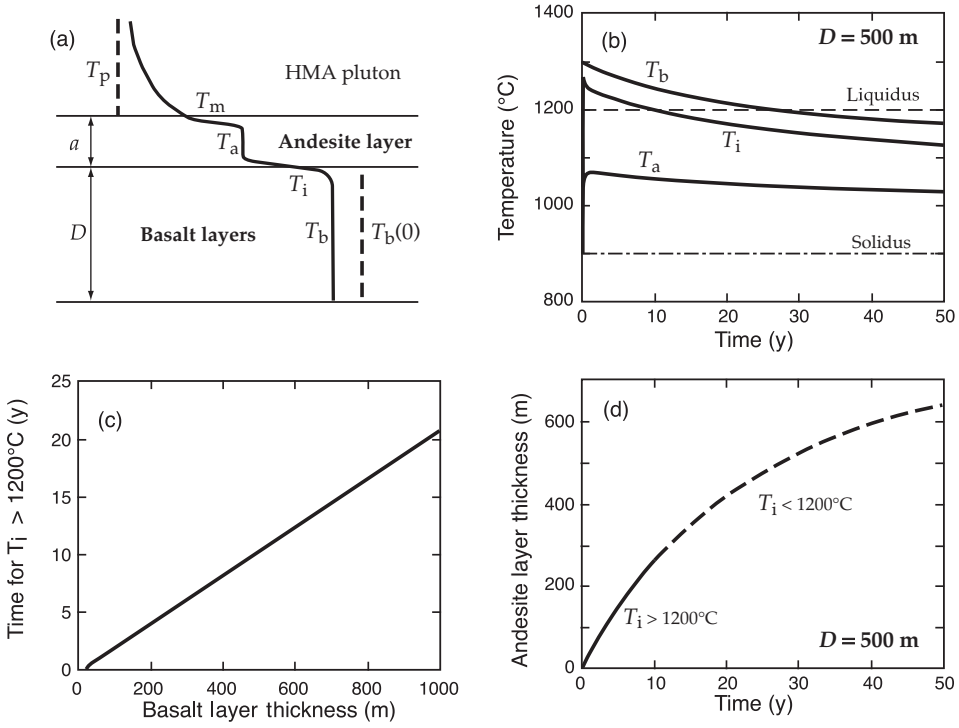

Fig. 16. Physical examination of remelting of an HMA pluton by intrusion of high-T basalt magma at its base. (a) Boundary conditions of a melting region at the base of the HMA pluton. The andesitic melt layer convects and has a uniform internal temperature. (b) Variation of the temperatures of the basaltic (T_b) and andesitic (T_a) magma layers with time for a 500 m sill emplaced into a 900°C HMA pluton. Secondary HMA magma can be produced at the base of the andesitic layer with T_i higher than the HMA liquidus (dashed line). (c) Time for production of secondary HMA melts with temperatures (T_i) higher than 1200°C as a function of the thickness of the basalt layer. (d) Variation of the thickness of the andesitic magma layer as a function of time.

ACKNOWLEDGEMENTS

We thank Satoru Nakashima and Satoshi Okamura for the FT-IR micro-spectrometer measurements, Yuka Yonezawa and Bogdan Vaglarov for analytical assistance, Miki Fukuda for preparing the manuscript and figures, and Monica Handler, James Brophy, Glen Gaetani and editor Dennis Geist for constructive comments on the manuscript.

REFERENCES

Arai, S. (1994). Compositional variation of olivine–chromian spinel in Mg-rich magmas as a guide to their residual spinel peridotites. *Journal of Volcanology and Geothermal Research* **59**, 279–293.

Ballhaus, C. G. (1993). Redox states of lithospheric and asthenospheric upper mantle. *Contributions to Mineralogy and Petrology* **114**, 331–348.

Ballhaus, C. G., Berry, R. F. & Green, D. H. (1990). Oxygen fugacity controls in the Earth's upper mantle. *Nature* **348**, 437–440.

Ballhaus, C. G., Berry, R. F. & Green, D. H. (1991). High pressure experimental calibration of the olivine–orthopyroxene–spinel oxygen geobarometer: implications for the oxidation state of the upper mantle. *Contributions to Mineralogy and Petrology* **107**, 27–40.

Burnham, C. W. & Nekvasil, H. (1986). Equilibrium properties of granite pegmatite magmas. *American Mineralogist* **71**, 239–263.

Chang, Q., Shibata, T., Shinotsuka, K., Yoshikawa, M. & Tatsumi, Y. (2003). Precise determination of trace elements in geological standard rocks using inductively coupled plasma mass spectrometry (ICP-MS). *Frontier Research on Earth Evolution* **1**, 357–362.

Couch, S., Sparks, R. S. J. & Carroll, M. R. (2001). Mineral disequilibrium in lavas explained by convective self-mixing in open magma chambers. *Nature* **411**, 1037–1039.

Crawford, A. J., Falloon, T. J. & Green, D. H. (1989). Classification, petrogenesis and tectonic setting of boninites. In: Crawford A. J. (ed.) *Boninites and Related Rocks*. London: Unwin Hyman, pp. 1–49.

Cribb, J. W. & Barton, M. (1997). Significance of crustal and source region processes on the evolution of compositionally similar calc-alkaline lavas, Mt. Hood, Oregon. *Journal of Volcanology and Geothermal Research* **76**, 229–249.

DePaolo, D. J. (1981). Trace element and isotopic effects of combined wallrock assimilation and fractional crystallization. *Earth and Planetary Science Letters* **53**, 189–202.

Dias, G. & Leterrier, J. (1994). The genesis of felsic–mafic plutonic associations: a Sr and Nd isotopic study of the Hercynian Braga granitoid massif (northern Portugal). *Lithos* **32**, 207–223.

Dobson, P. F. & O'Neil, J. R. (1987). Stable isotope compositions and water contents of boninite series volcanic rocks from Chichi-jima, Bonin Islands, Japan. *Earth and Planetary Science Letters* **82**, 75–86.

Eichelberger, J. C. (1975). Origin of andesite and dacite: evidence of mixing at Glass Mountain in California and at other Circum-Pacific volcanoes. *Geological Society of America Bulletin* **86**, 1381–1391.

Feeley, T. C., Cosca, M. A. & Lindsay, C. R. (2002). Petrogenesis and implications of calc-alkaline cryptic hybrid magmas from Washburn

Volcano, Absaroka volcanic province, USA. *Journal of Petrology* **43**, 663–703.

Furukawa, Y. & Tatsumi, Y. (1999). Melting of a subducting slab and production of high-Mg andesite magmas: unusual magmatism in SW Japan at 13~15 Ma. *Geophysical Research Letters* **26**, 2271–2274.

Gaetani, G. A., Grove, T. L. & Bryan, W. B. (1993). The influence of water on the petrogenesis of subduction-related igneous rocks. *Nature* **365**, 332–334.

Gill, J. B. (1981). *Orogenic Andesites and Plate Tectonics*. Berlin: Springer-Verlag.

Goto, A. & Tatsumi, Y. (1994). Quantitative analysis of rock samples by an X-ray fluorescence spectrometer (I). *The Rigaku Journal* **11**, 40–59.

Goto, A. & Tatsumi, Y. (1996). Quantitative analysis of rock samples by an X-ray fluorescence spectrometer (II). *The Rigaku Journal* **13**, 20–38.

Grove, T. L., Parman, S. W., Bowring, S. A., Price, R. C. & Baker, M. B. (2002). The role of an H_2O-rich fluid component in the generation of primitive basaltic andesites and andesites from the Mt. Shasta region, N California. *Contributions to Mineralogy and Petrology* **142**, 375–396.

Grove, T. L., Elkins-Tanton, L. T., Parman, S. W., Chatterjee, N., Münterner, O. & Gaetani, G. A. (2003). Fractional crystallization and mantle-melting controls on calc-alkaline differentiation trends. *Contributions to Mineralogy and Petrology* **145**, 515–533.

Hanyu, T., Tatsumi, Y. & Nakai, S. (2002). A contribution of slab-melts to the formation of high-Mg andesite magmas: Hf isotopic evidence from SW Japan. *Geophysical Research Letters* **29**, doi: 10.1029/2002GL015856.

Hildreth, W. (1981). Gradients in silicic magma chambers: implications for lithospheric magmatism. *Journal of Geophysical Research* **86**, 10153–10192.

Hildreth, W. & Moorbath, S. (1988). Crustal contributions to arc magmatism in the Andes of central Chile. *Contributions to Mineralogy and Petrology* **98**, 455–489.

Hirose, K. (1997). Melting experiments on lherzolite KLB-1 under hydrous conditions and generation of high-magnesian andesitic melts. *Geology* **25**, 42–44.

Hunter, A. G. (1998). Intracrustal controls on the coexistence of tholeiitic and calc-alkaline magma series at Aso Volcano, SW Japan. *Journal of Petrology* **39**, 1255–1284.

Huppert, H. E. (1986). The intrusion of fluid mechanics into geology. *Journal of Fluid Mechanics* **173**, 557–594.

Huppert, H. E. & Sparks, R. S. J. (1988*a*). Melting the roof of a chamber containing a hot, turbulently convecting fluid. *Journal of Fluid Mechanics* **188**, 107–131.

Huppert, H. E. & Sparks, R. S. J. (1988*b*). The generation of granitic magmas by intrusion of basalt into continental crust. *Journal of Petrology* **29**, 599–624.

Kay, R. W. (1978). Aleutian magnesian andesites: melts from subducted Pacific Ocean crust. *Journal of Volcanology and Geothermal Research* **4**, 117–132.

Kelemen, P. B. (1995). Genesis of high Mg-number andesites and the continental crust. *Contributions to Mineralogy and Petrology* **120**, 1–19.

Kinzler, R. J., Grove, T. L. & Recca, S. I. (1990). An experimental study on the effect of temperature and melt composition on the partitioning of nickel between olivine and silicate melt. *Geochimica et Cosmochimica Acta* **54**, 1255–1265.

Kuroda, N., Shiraki, K. & Urano, H. (1978). Boninite as a possible calc-alkalic primary magma. *Bulletin of Volcanology* **41**, 563–575.

Kushiro, I. (1969). The system forsterite–diopside–silica with and without water at high pressures. *American Journal of Science* **267-A**, 269–294.

Kushiro, I. & Sato, H. (1978). Origin of some calc-alkalic andesites in Japanese islands. *Bulletin of Volcanology* **41**, 576–585.

Marsh, B. D. (1989). Magma chambers. *Annual Review of Earth and Planetary Sciences* **17**, 439–474.

Matsui, Y., Onuma, N., Nagasawa, H., Higuchi, H. & Banno, S. (1977). Crystal structure control in trace element partition between crystal and magma. *Bulletin de la Société Française de Minéralogie et de Cristallographie* **100**, 315–324.

Matthews, S. J., Sparks, R. S. J. & Gardeweg, M. C. (1999). The Piedras Grandes–Soncor eruptions, Lascar Volcano, Chile: evolution of a zoned magma chamber in the Central Andean upper crust. *Journal of Petrology* **40**, 1891–1919.

Miyashiro, A. (1974). Volcanic rock series in island arcs and active continental margins. *American Journal of Science* **274**, 321–355.

Miyazaki, T., Shibata, T. & Yoshikawa, M. (2003). New synthesis method of silica-gel for lead isotope analysis. *Proceedings of the Japan Academy* **79B**, 58–62.

Moore, G., Vennemann, T. & Carmichael, I. S. E. (1998). An empirical model for the solubility of H_2O in magmas to 3 kilobars. *American Mineralogist* **83**, 36–42.

Murphy, M. D., Sparks, R. S. J., Barclay, J., Carroll, M. R. & Brewer, T. S. (2000). Remobilization of andesite magma by intrusion of mafic magma at the Soufriére Hills Volcano, Montserrat, West Indies. *Journal of Petrology* **41**, 21–42.

Nabelek, P. & Langmuir, C. H. (1986). The significance of unusual zoning in olivines from FAMOUS area basalt 527-1-1. *Contributions to Mineralogy and Petrology* **93**, 1–8.

Nakamura, M. (1995). Residence time and crystallization history of nickeliferous olivine phenocrysts from the northern Yatsugatake volcanoes, central Japan: application of a growth and diffusion model in the system Mg–Fe–Ni. *Journal of Volcanology and Geothermal Research* **66**, 81–100.

Okino, K., Shimakawa, Y. & Nagaoka, S. (1994). Evolution of the Shikoku Basin. *Journal of Geomagnetism and Geoelectrics* **46**, 463–479.

Okino, K., Kasuga, S. & Ohara, Y. (1998). A new scenario of the Parece Vela Basin genesis. *Marine Geophysical Researches* **20**, 21–40.

Okino, K., Ohara, Y., Kasuga, S. & Kato, Y. (1999). The Philippine Sea: new survey results reveal the structure and the history of the marginal basins. *Geophysical Research Letters* **26**, 2287–2290.

Otofuji, Y., Itaya, T. & Matsuda, T. (1991). Rapid rotation of Southwest Japan: palaeomagnetism and K–Ar ages of Miocene volcanic rocks of Southwest Japan. *Geophysical Journal International* **105**, 397–405.

Pearce, J. A., Van der Laan, S. R., Arculus, R. J., Murton, B. J., Ishii, T., Peate, D. W. & Parkinson, I. J. (1992). Boninite and harzburgite from Leg 125 (Bonin–Mariana forearc): a case study of magma genesis during the initial stages of subduction. In: Fryer, P., *et al.* (eds) *Proceedings of the Ocean Drilling Program, Scientific Results, 125*. College Station, TX: Ocean Drilling Program, pp. 623–659.

Roeder, P. L. & Emslie, R. F. (1970). Olivine–liquid equilibrium. *Contributions to Mineralogy and Petrology* **29**, 275–289.

Rorolo, S. G. & Castorina, F. (1998). Transition from mildly-tholeiitic to calc-alkaline suite: the case of Chichontepec volcanic centre, El Salvador, Central America. *Journal of Volcanology and Geothermal Research* **86**, 117–136.

Sakuyama, M. (1979). Evidence of magma mixing: petrological study of Shirouma-Oike calc-alkaline andesite volcano, Japan. *Journal of Volcanology and Geothermal Research* **5**, 179–208.

Sakuyama, M. (1981). Petrological study of the Myoko and Kurohime volcanoes, Japan: crystallization sequence and evidence for magma mixing. *Journal of Petrology* **22**, 553–583.

Sato, H. (1977). Nickel content of basaltic magmas: identification of primary magmas and a measure of the degree of olivine fractionation. *Lithos* **10**, 113–120.

Sato, H. & Banno, S. (1983). NiO–Fo relation of magnesian olivine phenocryst in high-magnesian andesite and associated basalt–andesite–sanukite from Northeast Shikoku, Japan. *Bulletin of the Volcanological Society of Japan* **28**, 141–156.

Saunders, A. D., Rogers, G., Marriner, G. F., Terrell, D. J. & Verma, S. P. (1987). Geochemistry of Cenozoic volcanic rocks, Baja California, Mexico: implications for the petrogenesis of post-subduction magmas. In: Weaver, S. D. & Johnson, R. W. (eds) *Tectonic Controls on Magma Chemistry*. Amsterdam: Elsevier, pp. 223–245.

Scowen, P. A. H., Roeder, P. L. & Helz, R. T. (1991). Reequilibration of chromite within Kilauea Iki lava lake, Hawaii. *Contributions to Mineralogy and Petrology* **107**, 8–20.

Shibata, K. (1978). Contemporaneity of tertiary granites in the outer zone of Southwest Japan. *Bulletin of Geological Survey of Japan* **29**, 51–54.

Shibata, T., Yoshikawa, M. & Tatsumi, Y. (2003). An analytical method for determining precise Sr and Nd isotopic compositions and results for thirteen rock standard materials. *Frontier Research on Earth Evolution* **1**, 363–367.

Shimoda, G., Tatsumi, Y., Nohda, S., Ishizaka, K. & Jahn, B. M. (1998). Setouchi high-Mg andesites revisited: geochemical evidence for melting of subducting sediments. *Earth and Planetary Science Letters* **160**, 479–492.

Shukuno, H. (2003). Quantitative analysis of rock-forming minerals and volcanic glasses by electron probe microanalyser. *Frontier Research on Earth Evolution* **1**, 129–136.

Sisson, T. W. & Grove, T. L. (1993). Experimental investigations of the role of H_2O in calc-alkaline differentiation and subduction zone magmatism. *Contributions to Mineralogy and Petrology* **113**, 143–166.

Sobolev, A. V. & Danyushevsky, L. V. (1994). Petrology and geochemistry of boninites from the north termination of the Tonga Trench: constraints on the generation conditions of primary high-Ca boninite magmas. *Journal of Petrology* **35**, 1183–1211.

Spencer, K. J. & Lindsley, D. H. (1981). A solution model for coexisting iron–titanium oxides. *American Mineralogist* **11–12**, 1189–1201.

Sumii, T. (2000). K–Ar ages of the Miocene Setouchi volcanic rocks in the western Setouchi Island Sea region, Southwest Japan. *Journal of the Geological Society of Japan* **106**, 609–619.

Sun, S. S. & McDonough, W. F. (1989). Chemical and isotopic systematics of oceanic basalts: implications for mantle composition and processes. In: Saunders, A. D. & Norry, M. J. (eds) *Magmatism in the Ocean Basins*. *Geological Society, London, Special Publications* **42**, 313–345.

Takahashi, E. (1990). Speculation on the Archean Mantle: missing link between komatiite and depleted garnet peridotite. *Journal of Geophysical Research* **95**, 15941–15954.

Tamura, Y. & Tatsumi, Y. (2002). Remelting of an andesitic crust as a possible origin for rhyolitic magma in oceanic arcs: an example from the Izu–Bonin arc. *Journal of Petrology* **43**, 981–1001.

Tamura, Y., Yuhara, M., Ishii, T., Irino, N. & Shukuno, H. (2003). Andesites and dacites from Daisen Volcano, Japan: partial-to-total remelting of an andesite magma body. *Journal of Petrology*, **44**, 2243–2260.

Tani, K., Kawabata, H., Chang, Q., Sato, K. & Tatsumi, Y. (2005). Quantitative analysis of silicate rock major and trace elements by X-ray fluorescence spectrometer: evaluation of analytical precision and sample preparation. *Frontier Research on Earth Evolution* **2**, in press.

Tatsumi, Y. (1981). Melting experiments on a high-magnesian andesite. *Earth and Planetary Science Letters* **54**, 357–365.

Tatsumi, Y. (1982). Origin of high-magnesian andesites in the Setouchi volcanic belt, Southwest Japan: II, Melting phase relations at high pressures. *Earth and Planetary Science Letters* **60**, 305–317.

Tatsumi, Y. (1983). Volcanic geology of the island of Shodo-Shima, Kagawa Prefecture, southwestern Japan, and its influence on the paleoenvironment of the area of the Seto Inland Sea. *Journal of the Geological Society of Japan* **89**, 693–706.

Tatsumi, Y. (2001). Geochemical modeling of partial melting of subducting sediments and subsequent melt–mantle interaction: generation of high-Mg andesites in the Setouchi volcanic belt, southwest Japan. *Geology* **29**, 323–326.

Tatsumi, Y. & Eggins, S. (1995) *Subduction Zone Magmatism*. Boston, MA: Blackwell Science, 211 pp.

Tatsumi, Y. & Hanyu, T. (2003). Geochemical modeling of dehydration and partial melting of subducting lithosphere: towards a comprehensive understanding of high-Mg andesite formation in the Setouchi volcanic belt, SW Japan. *Geochemistry, Geophysics, Geosystems* **4**, 1081, doi: 10.1029/2003GC000530.

Tatsumi, Y. & Ishizaka, K. (1981). Existence of andesitic primary magma: an example from Southwest Japan. *Earth and Planetary Science Letters* **53**, 124–130.

Tatsumi, Y. & Ishizaka, K. (1982*a*). Magnesian andesite and basalt from Shodo-Shima Island, Southwest Japan, and their bearing on the genesis of calc-alkaline andesites. *Lithos* **15**, 161–172.

Tatsumi, Y. & Ishizaka, K. (1982*b*). Origin of high-magnesian andesites in the Setouchi volcanic belt, Southwest Japan: I, Petrographical and chemical characteristics. *Earth and Planetary Science Letters* **60**, 293–404.

Tatsumi, Y. & Maruyama, S. (1989). Boninites and high-Mg andesites: tectonics and petrogenesis. In: Crawford, A. J. (ed.) *Boninites*. London: Unwin Hyman, pp. 50–71.

Tatsumi, Y., Ishikawa, N., Anno, K., Ishizaka, K. & Itaya, T. (2001). Tectonic setting of high-Mg andesite magmatism in the SW Japan Arc: K–Ar chronology of the Setouchi volcanic belt. *Geophysical Journal International* **144**, 625–631.

Tatsumi, Y., Nakashima, T. & Tamura, Y. (2002). The petrology and geochemistry of calc-alkaline andesites on Shodo-Shima Island, SW Japan. *Journal of Petrology* **43**, 3–16.

Tatsumi, Y., Shukuno, H., Sato, K., Shibata, T. & Yoshikawa, M. (2003). The petrology and geochemistry of high-Mg andesites at the western tip of the Setouchi volcanic belt, SW Japan. *Journal of Petrology* **44**, 1561–1578.

Tatsumi, Y., Shukuno, H., Yoshikawa, M., Chang, Q., Sato, K. & Lee, M. W. (2004). The petrology and geochemistry of volcanic rocks on Jeju Island: plume magmatism along the Asian continental margin. *Journal of Petrology* **46**, 523–553.

Taylor, R. N., Nesbitt, R. W., Vidal, P., Harmon, R., Auvray, B. & Croudace, I. W. (1994). Mineralogy, chemistry and genesis of the boninite series volcanics, Bonin Islands. *Journal of Petrology* **35**, 577–617.

Temel, A., Gündogdu, M. N. & Gourgaud, A. (1998). Petrological and geochemical characteristics of Cenozoic high-K calc-alkaline volcanism in Konya, Central Anatolia, Turkey. *Journal of Volcanology and Geothermal Research* **85**, 327–354.

Umino, S. & Kushiro, I. (1989). Experimental studies on boninite petrogenesis. In: Crawford A. J. (ed.) *Boninites*. London: Unwin Hyman, pp. 89–111.

van der Laan, S. R., Flower, M. F. J. & Groos, A. F. K. (1989). Experimental evidence for the origin of boninites: near-liquidus phase relations to 7·5 kbar. In: Crawford A. J. (ed.) *Boninites and Related Rocks*. London: Unwin Hyman, pp. 112–147.

Yamashita, S. (1999). Experimental study of the effect of temperature on water solubility in natural rhyolite melt to 100 MPa. *Journal of Petrology* **40**, 1497–1507.

Yogodzinski, G. M., Volynets, O. N., Koloskov, A. V., Seliverstov, N. I. & Matvenkov, V. V. (1994). Magnesian andesites and the subduction component in a strongly calc-alkaline series at Piip Volcano, far western Aleutians. *Journal of Petrology* **35**, 163–204.

Yoshikawa, M., Shibata, T. & Tatsumi, Y. (2001). The Sr, Nd and Pb isotopic ratios of GSJ standard rocks. *Annual Report of Beppu Geothermal Research Laboratory, Kyoto University* **FY2000**, 30.